Pretransitional Effects in Dimyristoylphosphatidylcholine Vesicle Membranes: Optical Dynamometry Study

R. Dimova,*† B. Pouligny,* and C. Dietrich*‡

*Centre de Recherche Paul-Pascal, Centre National de la Recherche Scientifique, 33600 Pessac, France; †Laboratory of Thermodynamics and Physicochemical Hydrodynamics, Faculty of Chemistry, Sofia University, Sofia 1164, Bulgaria; and ‡Department of Cell Biology and Anatomy, University of North Carolina, Chapel Hill, North Carolina 27599 USA

ABSTRACT We used micron-sized latex spheres to probe the phase state and the viscoelastic properties of dimyristoylphosphatidylcholine (DMPC) bilayers as a function of temperature. One or two particles were manipulated and stuck to a DMPC giant vesicle by means of an optical trap. Above the fluid-gel main transition temperature, $T_m \cong 23.4°C$, the particles could move on the surface of the vesicle, spontaneously (Brownian motion) or driven by an external force, either gravity or the laser beam's radiation pressure. From the analysis of the particle motions, we deduced the values of the membrane hydrodynamic shear viscosity, η_s, and found that it would increase considerably near T_m. Below T_m, the long-distance motion of the particles was blocked. We performed experiments with two particles stuck on the membrane. By optical dynamometry, we measured the elastic resistance of the membrane to a variation in the interparticle distance and found that it would decrease considerably (down to zero) when the temperature was increased to T_m. We propose an interpretation relating the elastic response to the membrane curvature modulus, k_C. In this scheme, the two-bead dynamometry experiments provide a direct measurement of k_C in the P'_β phase of lipid bilayers.

I. INTRODUCTION

Lipid bilayers are conventionally accepted to be the simplest model that approximates some properties of biological membranes. Besides their structural resemblance, they are characterized by physical properties similar to those of biomembranes, including thickness, water permeability, bending rigidity, surface tension, and viscosity. Furthermore, artificial lipid membranes are well-defined systems and are readily prepared. Thus they provide a unique opportunity to investigate certain physiological functions and processes in biological membranes. In addition, bilayers are convenient systems for investigating two-dimensional (2-D) molecular motion (Saffman, 1976) and ordering (Nelson and Halperin, 1979; Nelson and Peliti, 1987; Seung and Nelson, 1988).

It has been established that the biological membranes are not rigid bodies but flexible and fluid materials. However, the biomembrane lipids exhibit a range of phase transitions (from fluid liquid crystalline to gel-like structures). It is known that the so-called growth temperature of some microorganisms is closely related to the membrane phase transition. Phospholipid phase transitions could also be important in regulating the activities of membrane proteins and their interaction with the lipid matrix. For instance, the lipid bilayer should be "softer" and not very viscous, to permit easy structural reconfiguration of the protein molecule. The lipid bilayer, being in the fluid state, would allow an inclusion to move without restoring force. On the other hand, when frozen or when subjected to a large deformation, the biological membrane exhibits an elastic response (Hochmuth et al., 1980; Waugh and Evans, 1979) (the red blood cell membrane has often been modeled as a thin rubber sheet; see, for instance, Skalak et al., 1973).

In terms of molecular structure, membrane fluidity in the L_α phase implies "melted" hydrocarbon chains of the lipid and positional disorder of the molecules in the bilayer plane. Conversely, in gel phase the lipid bilayer becomes "stiff," the acyl chains freeze in a nearly all-*trans* configuration, and the molecules (heads and/or chains) are apparently arranged in a 2-D hexagonal lattice. Thus the phase state of the lipid bilayer largely influences the mechanical properties of the membrane itself. A large variety of techniques have been employed to study the phase transition behavior of bilayer systems on both molecular and on macroscopic scales: differential scanning calorimetry (Janiak et al., 1976, 1979; Koynova and Caffrey, 1998; Heimburg, 1998), x-ray diffraction (Janiak et al., 1976, 1979; Brady and Fein, 1977, Smith et al., 1988), Raman spectroscopy (see refs. in Pink et al., 1980), NMR (Davis, 1979; MacKay, 1981; Wittebort et al., 1981), electron spin resonance (Tsuchida and Hatta, 1988), spectroscopic techniques describing molecular diffusion (see refs. in Tocanne et al., 1994), ultrasonic studies (Mitaku et al., 1978), and micropipette techniques (Evans and Kwok, 1982; Needham and Evans, 1988; Needham and Zhelev, 1996).

Dimyristoylphosphatidylcholine (DMPC) is a frequently studied artificial lipid because it undergoes a phase transition at a convenient temperature. Upon cooling below ~23.6°C (Koynova and Caffrey, 1998) it undergoes a transition from the liquid crystalline L_α phase to the P'_β solid rippled phase, characterized by periodic corrugations of the bilayer. Studies on the microscopic level (electron spin

Received for publication 12 October 1999 and in final form 5 April 2000.

Address reprint requests to Dr. B. Pouligny, Centre de Recherche Paul-Pascal, CNRS, av. A. Schweitzer, 33600 Pessac, France. Tel.: 33-05-56-84-56-83; Fax: 33-05-56-84-56-00; E-mail: pouligny@crpp.u-bordeaux.fr.

0006-3495/00/07/340/17 $2.00

resonance, ^{13}C NMR) showed that a significant fraction ($\sim$20%) of chain disorder still exists in the P'_β phase (Davis, 1979; MacKay, 1981; Wittebort et al., 1981; Tsuchida and Hatta, 1988). Lateral diffusion measurements (Derzko and Jacobson, 1980) detected heterogeneity in the self-diffusion coefficient and interpreted the results by assuming the existence of fast and slow components differing by several orders of magnitude. It was suggested (Schneider et al., 1983) that the P'_β phase comprises bands of ordered lipid separated by bands of disordered ones, the latter coinciding with the regions of high curvature in the rippled structure (as also proposed by Tsuchida and Hatta, 1988). A recent study (Jutila and Kinnunen, 1997) on the DMPC phase transition in large unilamellar vesicles reported evidence of pretransitional phenomena that were correlated to structure fluctuations and gel-like domain formation. The complexity of the melting process in giant vesicles was visualized by two-photon fluorescence microscopy (Bagatolli and Gratton, 1999). Although numerous studies have been performed, information on the physical characteristics of the lipid bilayer in the phase transition region is still needed. The work reported here is aimed at better understanding the mechanical properties of the lipid membrane on a macroscopic level (note that among the techniques cited above, few work on this scale).

Our experiments deal with micron-sized latex beads attached to giant vesicle membranes. The particles are manipulated by means of an optical trapping system (Velikov et al., 1997). In their motion the latex spheres directly "feel" the state of the membrane. We use them as macroscopic mechanical probes to characterize the viscous or/and elastic responses of the vesicle membrane. The general problem of the friction experienced by a single particle when it moves along a fluid vesicle surface has been studied (Dimova et al., 1999a), and this has allowed deduction of the membrane shear viscosity (η_s) from the kinetics of particle motion. The general procedure (it is applicable to different particle and vesicle sizes and particle penetrations across the membrane) was tested with polystyrene latex beads and SOPC (L_α-stearoyl-oleoyl-phosphatidylcholine) membranes, which are fluid at room temperature.

In this work we study the DMPC membrane above and below the gel-fluid transition temperature. Basically, we investigate the temperature variation of the membrane viscosity in the fluid phase ($T > T_m$), using the above-mentioned single-bead method (Dimova et al., 1999a). In the gel phase ($T < T_m$), we probe the membrane elasticity by manipulating two beads simultaneously, and we measure the membrane elastic response by optical dynamometry up to T_m. As far as we know, these are the first experiments of that kind dedicated to lipid membranes and aimed at characterizing their pretransitional behavior on both sides of T_m. From the viewpoint of experimental techniques, ours has much in common with a number of recent experiments on biological membranes, using spherical particles as probes, either by optical (Bronkhorst et al., 1995; Hénon et al., 1999; see also Ashkin, 1997), or magnetic (Bausch et al., 1998, 1999; Boulbitch, 1999) dynamometry. All of these experiments are difficult to carry out and to interpret. An important point of this report is dedicated to interpreting the measured elastic response as a function of basic membrane elastic moduli. As we will explain, we do not read our data in terms of the membrane shear modulus (as one might believe a priori), but rather in terms of the membrane curvature modulus (k_C). In short, we report on the pretransitional behavior of k_C in the gel phase.

The paper is organized as follows. The next section (II) briefly introduces the materials and methods: sample preparation, experimental set-up, and procedure for the particle path analysis. In section III, we explain the principles of the different experimental methods and the kind of information that they provide. We start with the viscosimetry experiments: the procedures for measuring the particle friction coefficient and deducing the membrane viscosity are briefly reviewed in sections III.1 and III.2, respectively. The approach to the study of the gel phase elasticity, by optical dynamometry with two beads, is explained in section III.3. Our experimental results are reported in section IV: there we show the variation in η_s above T_m and that in the membrane stiffness (k_M) below T_m. The pretransitional behaviors of η_s and k_M are discussed and tentatively interpreted in section V. Our estimate of the amplitude of k_C in the gel phase is based not on a theory but on true analog simulations, which we carried out with macroscopic elastic sheets. These experiments are briefly described in the Appendix.

II. MATERIALS AND METHODS

II.1. Vesicle preparation

Giant vesicles were prepared from 1,2-dimyristoyl-*sn*-glycero-3-phosphocholine (DMPC) (Avanti Polar Lipids, Alabaster, AL; no additional purification of lipid was performed), using the method of electroformation (Angelova and Dimitrov, 1986; Angelova et al., 1992). During vesicle formation, the temperature (30°C) was kept well above the main phase transition of DMPC, and an electric field of a few V/mm was applied. The vesicles grow along platinum electrodes, on which the lipid was originally deposited. At the end of the preparation, the vesicles were usually interconnected and clustered. Target vesicles were selected at the outer rim of such clusters for experiments. There one easily finds vesicles that are unilamellar (as far as we can determine from phase contrast views) and without obvious internal structures. Most often, these outer vesicles were spherical and were connected just by a few contact points to the cluster. Sometimes they adhered by easily visible flat portions to neighbors or to the nearby platinum electrode.

The experimental cell is equipped with a circulating water jacket, allowing for a homogeneous temperature distribution in the chamber (see a detailed sketch in Fig. 1). The whole experimental unit is mounted on a motorized *x-y* stage. Basically, the optically trapped particles are immobile. To bring them in contact with vesicles, we moved the cell with the *x-y* stage. The temperature of the circulating water was kept constant to within $\pm$0.1°C by means of a cryothermostat (Lauda RM6) and measured by a thermocouple located inside the cell (see Fig. 1 *A*) (some of the experib-

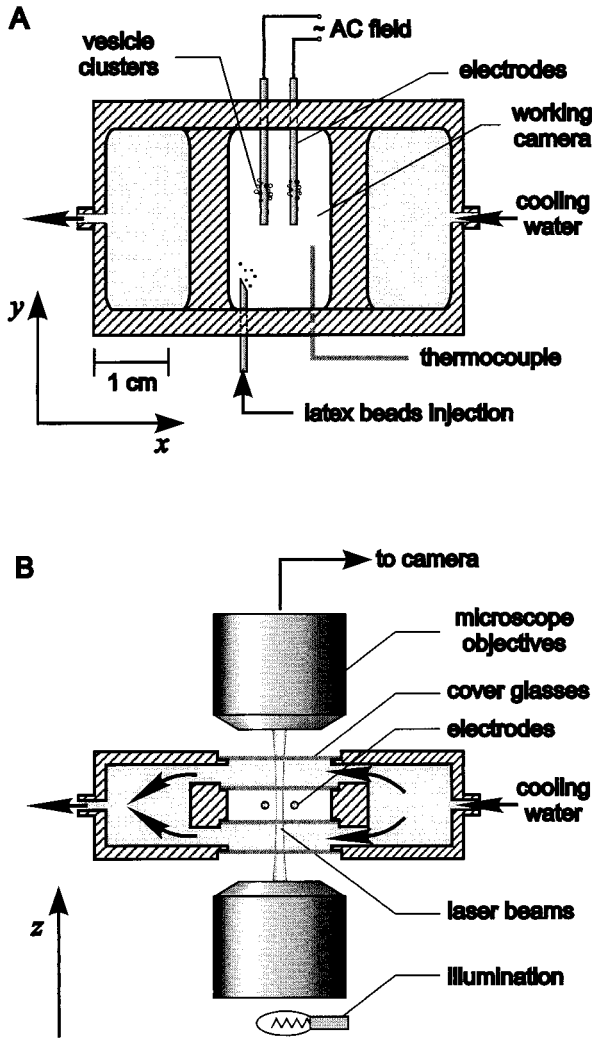

FIGURE 1 A schematic sketch of the experimental chamber. (*A*) Horizontal section: the cooling water cycle includes a cryothermostat. (*B*) Cross section: the optical trap is realized by two contrapropagating laser beams focused on the working cell by the two objectives.

ments reported were performed before construction of the chamber in Fig. 1, and the temperature was controlled only to within about ±0.4°C). The device can be operated from, say, 50°C down to ~15°C.

II.2. Optical manipulation of latex beads

The optical trap, specially designed to ensure a long working distance (on the *z* axis) between manipulated particles and optical components, has been described in detail elsewhere (Angelova and Pouligny, 1993; see also Dietrich et al., 1997, for additional characteristics of the set-up). Basically, the trap consists of two contrapropagating laser beams focused inside the experimental chamber (standard optical tweezers are created from a single sharply focused beam; see Ashkin et al., 1986).

For the experiments, we used latex spheres (Polyscience, Warrington, PA) with diameters ranging from 2 to 12 μm. To avoid contamination with lipid, the beads are injected at some distance ($\approx$ 15 mm) from the vesicle clusters at the electrodes (see Fig. 1 *A*). We pick up a particle with the laser trap and transport it to a previously selected vesicle. The bead sticks with a quick jump toward the vesicle interior as it comes in contact with the lipid bilayer. In our procedure, we attach the particle to the membrane in the fluid state, i.e., at $T > T_m$, but adhesion is possible below T_m as well. The way in which the particle stabilizes itself across the vesicle membrane is sometimes complex (see Dietrich et al., 1997, for details). A final equilibrium position is established within several seconds. This position is stable on the time scale of a single experiment (~1 h). By "stable" we mean that it does not change spontaneously and cannot be modified by the laser radiation pressure forces. When the lipid bilayer is in the fluid state, beads are allowed to move along the membrane. Driven by gravity, large and heavy beads sediment toward the bottom of the vesicle (see Fig. 2 *A*). Small and light particles exhibit Brownian motion (see Fig. 2 *B*). Beads can also be directed by the radiation pressure force (see Fig. 2 *C*). When the temperature is decreased below T_m, a membrane-bound particle becomes "frozen." It is no longer possible to make it move everywhere on the vesicle surface. Only a small lateral displacement can be achieved by means of the optical trap. When the laser beam is switched off, the particle returns to a point near its original position.

Particle size calibration is performed before adhesion to the vesicle. The bead sedimentation velocity, v_{sed}, was measured in bulk water. Application of Stokes' law yields the bead radius $a = (9\eta v_{sed}/2\Delta\rho g)^{1/2}$, where $\Delta\rho$ is the density difference between water and latex ($\approx$ 0.05 g/cm^3), g is the gravity acceleration, and η is the viscosity of water. For small particles, instead of measuring the sedimentation velocity, one can analyze their Brownian

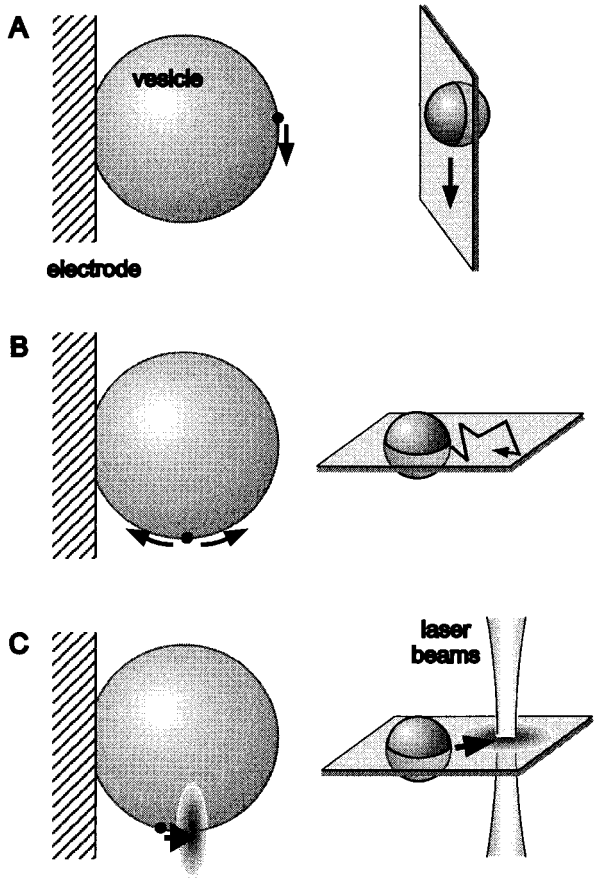

FIGURE 2 Schematic illustrations representing three different approaches to measurement of the mobility of a particle bound to a membrane. (*A*) Gravity-driven sedimentation. (*B*) Brownian motion at the bottom of the vesicle. (*C*) Optical trapping kinetics (the sketch is exaggerated in terms of distances).

motion. Extracting the diffusion coefficient in the bulk aqueous suspension (D_{free}) provides the bead radius from the Stokes-Einstein equation [$a = k_BT/(6\pi\eta D_{free})$], where k_BT is the Boltzmann energy.

The calibration of the optical trap forces is described in the next subsection. For the latex spheres of interest, no heating effects (absorption) were detected (Angelova and Pouligny, 1993). The applied laser powers were weak (less than 6 mW in the sample cell) compared with experiments with optical tweezers, in which the highly focused laser spot (a few hundred mW) could induce heating of the lipid membrane (Liu et al., 1995) or even mechanical effects (Granek et al., 1995; Bar-Ziv et al., 1995).

For two-bead experiments a double trap configuration of the optical system is used. The laser beam is split into two pairs forming two traps (Angelova and Pouligny, 1993; Martinot-Lagarde et al., 1995). One trap is fixed, while the other can be moved by means of a mirror mounted on a one-direction motorized stage. The distance between the two traps can be adjusted between 0 and ~35 μm.

II.3. Optical dynamometry

The force (several pN) exerted on a trapped bead depends on its size and on the refractive indices of the particle and of the surrounding media; it is proportional to the applied laser power. Radiation pressure forces are directed through the center of the manipulated (supposedly spherical) particle (Martinot-Lagarde et al., 1995; Polaert et al., 1998). The radiation pressure for the beam geometry used was computed with the Generalized Lorenz-Mie Theory (GLMT) (Gouesbet et al., 1988; Ren et al., 1994; Martinot-Lagarde et al., 1995). In bulk water, the trap force in the *x-y* plane (transverse force component) is roughly proportional to the distance ($\bar{x}$) between the bead center and the beam axis, when it is less than ~0.6 times the particle radius, a (the deviation is within ±10%, which is a reasonable accuracy for the data interpretation, keeping in mind the experimental error). Fig. 3 presents the theoretically computed transverse optical trapping force, F_{RP}, versus $\bar{x}$ (the force is calculated for an incident laser power of 5 mW, which is a typical value). Different curves correspond to different particle radii.

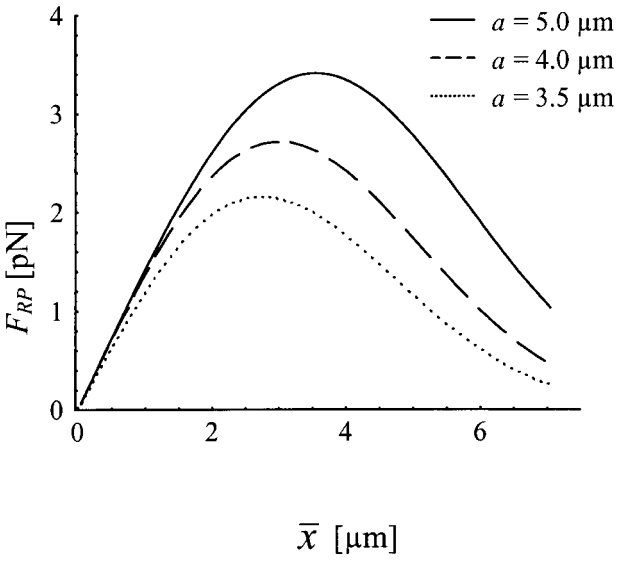

FIGURE 3 Numerical calculations of optical trap force, F_{RP} (transverse force component), as a function of particle off-centering, $\bar{x}$, for beads of different sizes. The computations are performed for the trap configuration used in experiments and an applied laser power of 5 mW. The wavelength of the incident beam is 514 nm in air; the beam waist is 4.15 μm.

Another method for deducing the magnitude of F_{RP} is to submit the trapped sphere to a constant counterflow of known velocity and determine the "escape" velocity, v_{esc}, at which the particle leaves the trap. The corresponding trapping force, which is the maximum of $F_{RP}(\bar{x})$, exactly balances the viscous drag force (Stokes' law):

$$F_{RP}^{max} = 6\pi a\eta v_{esc}. \quad (1)$$

Both methods were used to estimate the trapping force.

Knowing the radiation pressure force applied through the particle center, we probed the vesicle membrane for forces in the piconewton range. At temperatures at and above T_m, we measured the bilayer shear viscosity. Below T_m, by means of the two-particle manipulation, the elastic restoring force was studied.

II.4. Image processing

A classical microscope with elements integrated in the optical trap set-up allows us to observe bead and vesicle position from above (top view). While the vesicle contour and a small sphere (<4 μm in diameter) are best represented in phase-contrast mode, larger beads are preferably imaged in simple transmission (amplitude contrast) mode. Applying digital image processing allows the bead motion (horizontal projection) to be followed with a rate of ~6 Hz. Essentially, the algorithm is based on subtraction of a previously recorded background frame (without particle) and discrimination of the resulting image in 0 (no particle) and 1 (particle) levels. The accuracy is set by the pixel resolution (0.156 × 0.159 μm) of the CCD camera (Hamamatsu). Image sequences are recorded with standard video equipment (U-matic; SONY).

III. EXPERIMENTAL PROCEDURES AND DATA ANALYSIS

III.1. Viscosimetry of fluid membranes

In this subsection we discuss three different one-bead-one-vesicle scenarios followed in our experiments and their interpretations. By these single-particle manipulations, we determine the viscosity of the lipid bilayer in the fluid state ($T \geq T_m$). The parameter measured in all three experiments is the friction coefficient, ζ. It relates the bead velocity (v) and the drag force (F_{fr}) experienced by the particle:

$$F_{fr} = \zeta v. \quad (2)$$

The particle motion can be driven by gravity (sedimentation experiment, Fig. 2 *A*), by thermal fluctuations (Brownian motion, Fig. 2 *B*), or by radiation pressure force (Fig. 2 *C*). We suppose that the friction coefficient is constant when the membrane is in the fluid state. This amounts to hypothesizing that the bilayer shear viscosity is constant, i.e., independent of frequency. As we will see, the experimental results are in line with this assumption.

III.1.1. Sedimentation

After a particle becomes attached to the membrane, we bring it close to the upper pole of the vesicle and release it. The bead starts to glide down and approaches the lowest point at $\theta = \pi$ (Fig. 4 *A*). We observe the bead movement from above. Fig. 4 *B* shows a top view of a recorded particle trajectory. The driving force is gravity, projected onto the membrane. Sedimentation velocities are typically a few microns per second. Inertial contributions can be neglected (highly damped motion). The equation of motion is

$$0 = \tilde{m}g \sin\theta - \zeta\tilde{R}\dot{\theta}, \quad (3)$$

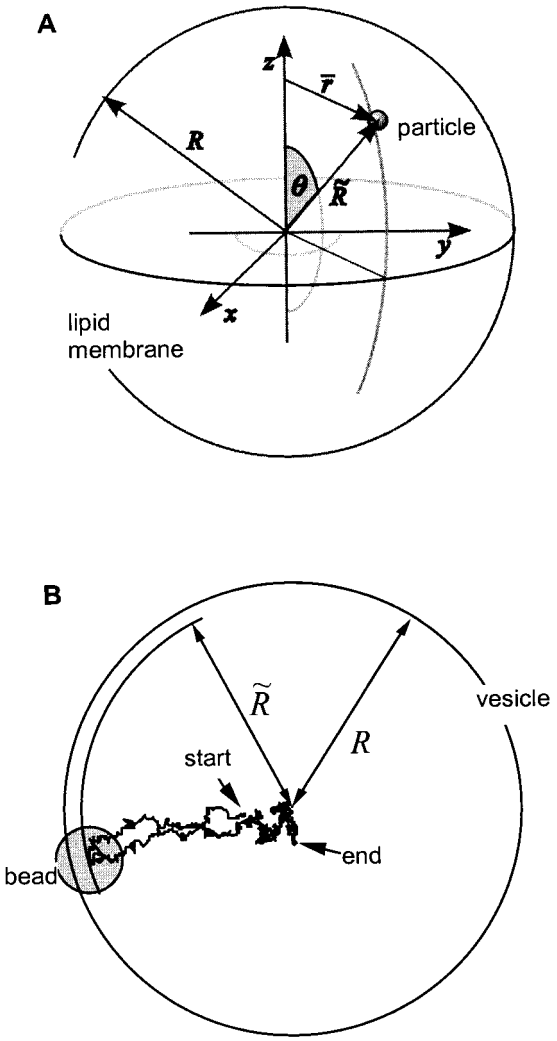

FIGURE 4 (*A*) The sketch illustrates the particle (latex bead) movement along the spherical surface of a vesicle; see text for notations. (*B*) A recorded particle trajectory, top view (the bead contour corresponds to the moment when the particle passes through the equatorial plane of the vesicle). The recorded trace is the horizontal projection of the particle path.

where $\tilde{m}g$ is the particle weight corrected for buoyancy. Note that the distance between the particle and the vesicle centers, $\tilde{R}$, may differ slightly from the vesicle radius R (see Fig. 4 *B*). Equation 3 is easily integrated in spherical coordinates:

$$f[\theta(t)] = f(\theta_0) - \tilde{m}gt/(\tilde{R}\zeta), \tag{4}$$

where $f(\theta) = \text{arctanh}(\cos\theta)$ and θ_0 is the particle position at time $t = 0$. The slope of the experimental time dependence of f yields the value of the friction coefficient, ζ. The solution of Eq. 3 for the horizontally projected (in the x-y plane) distance $\bar{r}$, between the particle and the vesicle centers, which is the directly measured parameter in our experiments, is

$$\bar{r}(\bar{t}) = \tilde{R}\sin\{2\arctan[\exp(\bar{t})]\tan(\theta_0/2)\}, \tag{5}$$

where $\tilde{t} = \tilde{m}gt/(\zeta\tilde{R})$. Equation 5 provides a master curve, representing the sedimentation path for any experimental geometry. However, as previously discussed (Velikov et al., 1997, 1999), working with Eq. 5 is justified only in the zone of the vesicle equator ($\theta = \pi/2$), provided the particle is heavy enough. When the latex bead is close to a pole of the vesicle, the effective gravitation force projected onto the vesicle surface approaches zero and Brownian excursions may become significant. Near the equator of the vesicle the drift velocity, v, is at maximum, $v_{\max} = \tilde{m}g/\zeta$. The condition for a "heavy enough" particle is defined by the so-called Peclet number, $\text{Pe} = \tilde{m}g\tilde{R}/(k_BT)$. Pe is a measure of the sedimentation contribution relative to thermally driven diffusion. In the limit of infinitely large values of Pe we end up with the purely mechanical problem set out in Eq. 5. In the high temperature limit ($\text{Pe} \to 0$) thermally induced fluctuations in the experimental sedimentation path become substantial. In fact, the applicability of Eqs. 3–5 depends on θ and is set by $\text{Pe}\sin\theta$. Our analysis of experimental trajectories, using Eq. 5 applied to the measured curves, was restricted to an interval in θ ($\pi/3 < \theta < 2\pi/3$) and $\text{Pe} > 100$.

III.1.2. Brownian motion

For smaller particles ($a < 2\ \mu$m) or small Pe numbers, the determination of ζ from sedimentation is problematic, and analyzing the Brownian excursions is more appropriate. In this case, we measure D, the particle diffusion coefficient, which is related to ζ by the Einstein-Stokes equation, $D = k_BT/\zeta$. Guiding the particle to the bottom of the vesicle and switching the optical trap off, one observes a random walk, which at first glance resembles 2-D motion. The diffusion constant can be extracted by studying the mean squared displacement of the particle in the short time limit. For Brownian diffusion in a flat plane this results in a straight line, $\langle(\Delta x)^2 + (\Delta y)^2\rangle = 4D\Delta t$. An essential difference from a free random walk along a horizontal plane is the fact that in the long time regime, gravity keeps the particle near the lowest point of the vesicle. Because the bead is bound to a spherical surface, the bead motion can be presented as taking place at the bottom of a parabolic potential well. The lateral extension, $\tilde{x}$, of the statistical cloud of particle positions is given by $k_BT \cong \tilde{m}g\tilde{x}^2/(2\tilde{R})$. If we release the particle at time $t = 0$ at $x = 0$ (the bottom of the well), the Brownian motion will be in the planar regime as long as $t \ll \tilde{t}$, where $\tilde{t}$ is defined by $\tilde{x}^2 = 4D\tilde{t}$. Finally $\tilde{t} = \tilde{R}\zeta/(2mg)$. In our experimental conditions, $\tilde{t}$ is on the order of 100 s at room temperature. In the long time regime, the averaged squared displacement must reach an equilibrium level. For our set-up with a detection rate of ~6 Hz, the planar regime lasts for 1 s ($\Delta t \leq$ 1s) or more and is clearly identified. In fact, this condition is satisfied in our experiments. The concepts of our Brownian motion analyses have been verified by computer simulations (Velikov et al., 1999). We also performed an additional experimental check of the values we obtained for the particle diffusion coefficient: the mobile x-y stage on which the experimental sample is mounted, was programmed so that its motion would simulate random Brownian displacement. We recorded the "motion" of particles that were "frozen" inside the sample cell (this condition was realized by replacing the water with a water-agarose gel). The data analyses yielded the correct value of D.

III.1.3. Optical trapping dynamics

As already commented, for distances to the trap origin smaller than ~0.6 a (see Fig. 3), the transverse radiation pressure force exerted on a latex bead increases linearly with the distance between the bead and trap centers: $F_{RP} \cong k_{RP}\bar{x}$ (the limit of the assumed linearity depends on the required accuracy of the value of F_{RP}). The coefficient k_{RP} or the trap "spring" constant depends on the bead size, beam geometry, and the laser power and is easily held constant for a series of experiments performed with the same bead.

We perform simple "catch experiments." The particle is brought to the bottom (or top) of the vesicle, where the lipid membrane is essentially perpendicular to the laser beams. The trap is switched off and repositioned a few microns to the side. When the trap is switched on again, the bead is attracted to the trap center. For displacements that are small compared to

the vesicle radius, the membrane can be regarded as flat and the bead as moving approximately in a straight line toward the trap. We neglect effects due to gravity. The equation of motion is

$$0 = k_{RP}\bar{x} - \zeta\dot{\bar{x}}. \quad (6)$$

The solution is

$$\bar{x}(t) = \bar{x}_0 \exp(-t/\tau_c), \quad (7)$$

where $\bar{x}_0$ is an integration parameter, representing the particle-trap distance at time $t = 0$ (after the trap repositioning); $\tau_c = \zeta/k_{RP}$ is the characteristic time of the process. The value of the radiation pressure constant, k_{RP}, is either deduced from GLMT calculations or estimated from the escape velocity measurements (see Eq. 1; roughly, $k_{RP} \cong 6\pi\eta v_{esc}$). For our experiments, the radiation pressure constant is on the order of 10^{-3} dyn/cm. Knowing k_{RP}, one can determine the friction coefficient, ζ, from an exponential fit to the measured distance $\bar{x}$.

We end this paragraph with a remark about Eq. 6. Following the same reasoning as for the sedimentation equation (Eq. 3), we expect Eq. 6 to be valid whenever the relevant Peclet number is large. Here we may put $Pe = E_{RP}/(k_BT)$, where E_{RP} is the particle optical trapping energy. E_{RP} is on the order of $a\Phi/c$, where Φ is the laser power acting on the particle and c is the velocity of light. With $\Phi = 5$ mW, a typical power, and $a = 2$ μm, we thus find $Pe \approx 10^4$. This proves that Brownian excursions are negligible in the particle trapping kinetics and that Eq. 6 can be safely applied.

III.2. From particle friction to membrane viscosity

Deducing the value of the membrane shear viscosity, η_s, from that of ζ necessitates a theory for the particle motion. We used the theory of Danov et al., either in the simple version for flat Langmuir films (Danov et al., 1995) or in the recent general version for vesicles (Danov et al., manuscript submitted for publication). As discussed by Danov et al. (manuscript submitted for publication) and Dimova et al. (1999a), two important assumptions of the theory are that the membrane behaves like a single film and that the membrane-particle contact line is locked on the particle surface ("contact line pinning"). These two assumptions greatly simplify the theory, and it was shown by Dimova et al. (1999a) and Dietrich et al. (1997) that they are satisfied by the latex bead-lipid vesicle system, indicating that the particle does not roll on the membrane and that lipids do not slip along the particle surface.

In the case of a small particle on a large vesicle the bead "sees" the membrane as a flat surface. For such systems, η_s can be simply deduced from the friction coefficient, ζ, following the procedure of Velikov et al. (1997). There the theory of Danov et al. (1995) was employed for the ζ-to-η_s inversion: the model for the motion of a particle along a flat infinite film at the air/water surface is adapted to a particle moving along a membrane (i.e., water/bilayer/water interface). The adaptation requires 1) that the bead be much smaller than the vesicle size, $a \ll R$ (to satisfy the condition for a flat surface), and 2) that the membrane intercept the particle through its equator, i.e., the contact angle has to be $\sim 90°$ (to allow for a superposition of two equivalent air/water systems).

For a large particle and an arbitrary radial penetration (or an arbitrary contact angle) of the particle, one needs to account for possible finite size effects (e.g., increased friction due to recirculation of the water enclosed in the vesicle bulk); a generalized theory accounting for these factors is available (Danov et al., manuscript submitted for publication). For membranes of moderate surface viscosity (e.g., on the order of 5×10^{-6} surface poise) the recirculation effect may have a considerable impact on the value of ζ. Indeed, the theory shows that ζ definitely increases beyond ζ_∞, the value corresponding to the flat membrane limit ($R/a \to \infty$), when $R/a < 10$ and when the particle penetrates more toward the vesicle interior. The theory was successfully applied to the interpretation of data from sedimentation and diffusion measurements (Dimova et al., 1999a) and allowed for a robust determination of the shear surface viscosity. For SOPC lipid membranes at room temperature, η_s was found to be $\sim 3 \times 10^{-6}$ surface poise (dyn·s/cm or sp; note that the commonly used "surface shear viscosity" has units of [bulk membrane viscosity $\times$ membrane thickness]).

The geometry of some of the experimental systems reported here permits application of the mathematically simpler model (Velikov et al., 1997). For others (e.g., when the bead is predominantly situated on one side of the vesicle surface), it was necessary to introduce a finite-size correction factor deduced from the theoretical predictions (Danov et al., manuscript submitted for publication). However, for measurements on highly viscous membranes (at temperatures close to T_m), we did not correct the raw data because the finite size correction was within experimental error.

III.3. Gel phase elastic response

III.3.1. Static elasticity

The static elastic experiment is carried out with a double trap configuration of the laser beams (see Fig. 5). An optimal bead radius for facile double trap manipulation is ~ 5 μm. Two particles are brought into contact with a previously selected vesicle in the fluid phase ($T > T_m$). Relatively large vesicles (generally $R > 40$ μm) are used, so that the adherent beads see the membrane as almost flat. It was preferable to work with vesicles having a

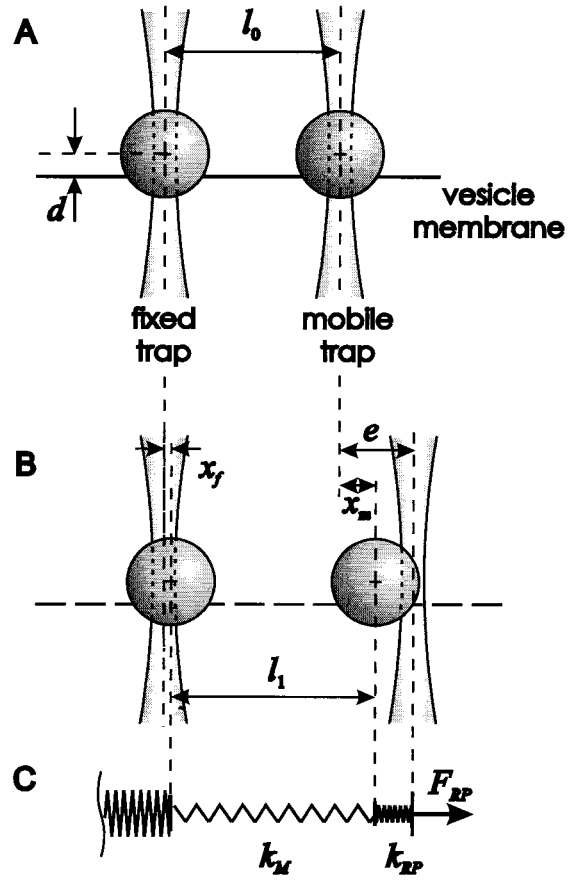

FIGURE 5 Experimental steps in the static elasticity experiment. $d = R - \tilde{R}$ indicates the particle penetration depth (d is positive when the particle center is external to the membrane surface). (*A*) Initial position of particles. (*B*) Mobile trap displacement. (*C*) "Three-spring" model.

visible contact area with the platinum electrode. In fact, vesicles having just a few contact points with neighbors easily detach from the cluster when they become gelled below T_m (Bagatolli and Gratton, 1999), whereas well-attached vesicles do not move. After beads have been stuck to the membrane, the chamber is cooled down to ~15°C, well below the main phase transition temperature of the lipid. The two beads become frozen across the membrane (usually beads were of equal penetration depth, d ; see Fig. 5 *A* for the definition of d) at a distance from each other that is determined by the two trap positions. The consecutive experimental steps are sketched in Fig. 5. The initial interparticle distance, which is the distance between the fixed and the mobile traps, is l_0 (Fig. 5 *A*). While keeping the temperature constant ($T < T_m$), we displace the mobile trap by a distance e. The new distance between the optical trap axes is then $l_0 + e$ (Fig. 5 *B*). In response to this perturbation, both particles move; the new interparticle distance is l_1. If the experiment was carried out in the fluid phase, we would have $l_1 = l_0 + e$, because the particles would lock on the beam axes. In the gel phase, the membrane elasticity acts against an increase in the particle separation, and then $l_1 < l_0 + e$. We denote the displacement of each particle, relative to its initial position, by x_f and x_m, for the beads in the fixed and mobile traps, respectively (see Fig. 5 *B*). We have

$$x_m - x_f = l_1 - l_0. \tag{8}$$

To analyze the bead-vesicle equilibrium, we use the three-spring model shown in Fig. 5 *C*. The membrane elastic resistance is represented by a spring of stiffness k_M. The two optical traps act like springs of stiffness k_{RP}. In this situation, the force balance equations read

$$k_{RP}x_f = k_M(l_1 - l_0), \tag{9a}$$

for the "f-bead" and

$$k_{RP}(e - x_m) = k_M(l_1 - l_0), \tag{9b}$$

for the "m-bead." Equations 8 and 9 yield

$$(l_1 - l_0)(2k_M + k_{RP}) = ek_{RP}. \tag{10a}$$

In this model, we have $e - x_m = x_f$, from symmetry. In the experiments reported in this article, we noticed that x_f was much smaller than x_m; in other words, the bead in the fixed trap moved less than that in the mobile trap. This nonsymmetrical behavior is most probably due to a nonsymmetrical repartition of the vesicle connections to the electrode and to the neighboring vesicles.

If we keep the f-bead immobile ($x_f = 0$), we have $x_m = l_1 - l_0$, and Eq. 9b gives

$$(l_1 - l_0)(k_M + k_{RP}) = ek_{RP}. \tag{10b}$$

Because $x_f < x_m$, we chose to analyze our data for k_M by following Eq. 10b. Nevertheless, note that the values of k_M given by Eqs. 10a and 10b differ by only a factor of 2. As we propose in paragraph V.2, k_M is roughly proportional to k_C, the membrane curvature elastic modulus. By "roughly" we mean a proportionality relation that holds only within a factor of 2 or so. In this context, it is not very important to decide which of Eq. 10a or Eq. 10b is the better model.

In the experiment, we measure $l_1 - l_0$ at a given temperature after ~15 min of equilibration time. Then the temperature is increased by 0.1°C and the sample is again left at rest for 15 min. Knowing the radiation pressure constant allows us to build the temperature dependence of k_M when the lipid is in the gel phase. The experiment terminates when the phase transition temperature is reached. At T_m, no elastic response is detected ($k_M = 0$), the membrane becomes fluid, and the particles readily follow the trap displacement. The chamber is then cooled down again, and the procedure is repeated. Measurements during different heating cycles, as well as on different particle-vesicle systems, give reproducible results within experimental error. The accuracy of k_M measurements noticeably decreases for low temperatures ($T < 19$°C) because the detected particle displacements approach the pixel resolution of the camera. Bead motion is hampered by the solidified membrane.

Equation 10b suggests a linear dependence of $l_1 - l_0$ as a function of e. This can be verified from experiments performed with different mobile trap displacements, e. To illustrate this point, we anticipate some of the results to be presented in the next section. Experimental results of the test are shown in Fig. 6. Different symbols correspond to measurements at different temperatures. The slopes of the linear fits to data give $k_{RP}/(k_M + k_{RP})$ and are adequate down to ~20.5°C. The solid line is of slope 1 and corresponds to $k_M = 0$ at $T \geq T_m$. Below 20.5°C, the data are too scattered to measure a slope. In principle, one might expect two sources of nonlinearity in the experimental $l_1 - l_0$ versus e data: 1) the radiation pressure forces are linear only for small particle displacements, and 2) the membrane elasticity is nonlinear when the interparticle distance is large. As we mentioned, x_f is generally very small, and essentially $x_m \cong l_1 - l_0$. Nonlinearity source 1 then mainly concerns the distance $e - x_m$, which should be less than ~0.6a. This sets a lower straight boundary, $l_1 - l_0 = e - 0.6a$, in Fig. 6 (as commented, the linearity limit $\bar{x} < 0.6a$ for F_{RP} is approximate; the lower boundary of the zone in Fig. 6 therefore is only a guide for the eye). The other source of nonlinearity (2) is more difficult to quantitatively set out. It is expected that when $l_1 - l_0$ is larger than some boundary, the $l_1 - l_0$ versus e dependence becomes nonlinear. Because there is no obvious tendency of that kind in the graph, the membrane response is apparently linear.

III.3.2. Dynamic elasticity

A complement to the two-particle procedure is to observe the system relaxation after a perturbation when the lipid is in the gel phase. We alter (stretch or shrink) the interparticle distance, l, by displacing the bead in the mobile trap to a new position. Then the mobile trap is switched off, thus releasing the particle. The bead relaxation motion back to its initial location is recorded in time. The temperature is kept constant throughout a single measurement and is varied for different experiments.

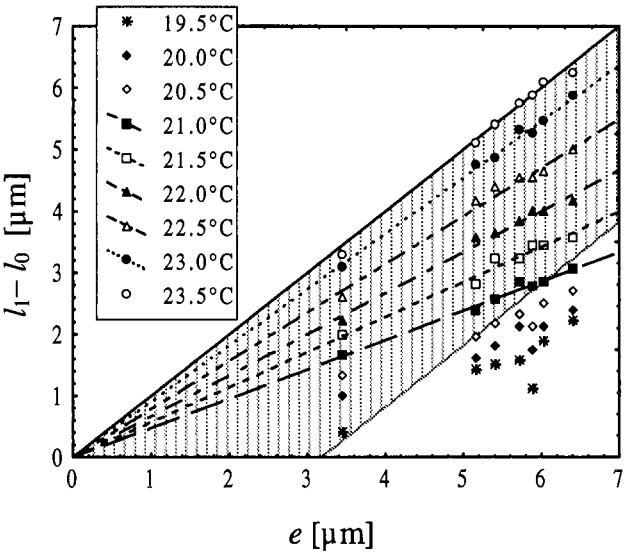

FIGURE 6 Test for linearity. The hatched zone covers the area of applicability of the spring model (the lower boundary is approximate). The broken lines are linear fits (least squares) to data at different temperatures (see legend). The slope of the solid line is 1.

One may suppose that the friction experienced by the relaxing particle is characterized by an effective friction coefficient ζ_{eff}. Then the simple approach of the "spring" model (Fig. 5 *C*) yields

$$l = A + B\exp(-t/\tau_r), \tag{11}$$

where A and B are constants and τ_r is the characteristic time of the membrane relaxation process, $\tau_r = \zeta_{eff}/(2k_M)$. Because the value of the stiffness constant, k_M, is known from the static elasticity experiments, one may deduce the effective friction coefficient, ζ_{eff}, from an exponential fit to the interparticle distance versus time.

IV. RESULTS

All five experimental techniques described in the previous section focus on studying the temperature dependence of membrane viscoelastic characteristics. The viscous resistance enters the theoretical descriptions of the experiments through the friction coefficient ζ. The elastic response below T_m is interpreted by introducing the effective spring constant k_M. In the following section we present results on these two characteristic parameters and demonstrate the temperature dependence of the membrane behavior in the region of the phase transition.

IV.1. Fluid membrane viscosity

For a membrane in the fluid phase, the three different viscosimetry methods that we presented in section III.1 are equivalent. This can be tested with the same particle. The bead has to be big enough to show a clear sedimentation path and, on the other hand, small enough to show Brownian excursions significantly larger than the resolution of the digital image processing. The following results concern one vesicle/particle system ($a = 3.2\ \mu$m, $R = 21\ \mu$m, $d = -0.2a$; see Fig. 5 *A* for the penetration d) where the bead satisfies these conditions.

Fig. 7 *A* presents two examples of sedimentation paths at two different temperatures. For the region $\bar{r}(t) > \tilde{R}/2$, the measured sedimentation trajectories are well described by Eq. 5 (Pe $\approx$ 340). The experimental data fit provides the maximum sedimentation velocity, v_{max}. The latter is inversely proportional to the particle friction coefficient. For the two examples presented in Fig. 7 *A*, the temperature decrease ($\Delta T = -0.7$°C) induces a ~20-fold increase in ζ.

The Brownian motion of the same particle was studied at the lower pole of the vesicle. The corresponding averaged squared displacements are given in Fig. 7 *B*. The slopes of the line fits (*solid lines*) for $\Delta t \leq 1$ s yield values for the diffusion coefficient. Similar to the case with sedimentation, decreasing the temperature considerably slows the Brownian motion.

Finally, Fig. 7 *C* shows the optical trapping kinetics of the same particle, in displacement, $\bar{x}$, versus t presentation. The time origin is defined as the instant when the trap is switched on. In the region $x < 0.6a$, the recorded trajectories are found to be exponential (Eq. 7). The characteristic time of the process, τ_c (fit parameter), shows a 25-fold increase when T is decreased from 23.3°C to 22.5°C.

The results of all experiments, performed with the same particle-vesicle system at different temperatures in the 22.5–28°C range are gathered in Fig. 8. Different symbols correspond to sedimentation (*diamonds*), Brownian motion (*filled squares*), or optical trapping dynamics (*asterisks*). While errors of sedimentation and diffusion experiments were estimated from the precision of the applied fits, trapping dynamics experiments were repeated at least six times, and the observed standard deviation was taken as a measure for the error. In all performed experiments, starting from higher temperatures and passing through the main phase transition, we observe a drastic decrease of particle mobility (i.e., increase in ζ). This drop is due to the well-known main phase transition of DMPC. In the fluid phase (>24°C) data from the three different methods are in fairly good agreement. For temperatures below ~22.5°C, no long-range particle movement was detected, which is a direct experimental indication that the lipid membrane became solid. Short-distance motion is still possible if the membrane is elastic enough (small elastic moduli) in the gel-like phase. Indeed, at 22°C we clearly detected an elastic response to optical bead displacements, and we observed short-range displacements caused by thermal agitation (hindered Brownian motion). Consequently, scattering of data near T_m for the three different methods might be the result of different sensitivities to partial elastic and/or restrained bead movement. Disappearance of the long-distance motion (when in sedimentation $\zeta \rightarrow \infty$) is the best criterion for locating T_m.

Instead of gathering the results of three different techniques with one and the same particle-vesicle system, as we did in Fig. 8, we now show the results obtained with three different particle-vesicle systems with the same technique, e.g., sedimentation. The surface viscosity is calculated using the procedure explained in section III.2. In two of the systems, the particles penetrated the vesicle, so that the flow confinement effect could not be neglected. In these cases it was necessary to use the full theory (Danov et al., manuscript submitted for publication) to correctly deduce η_s from ζ. It is evident from Fig. 9 that the three systems give coherent results. Far above the transition temperature, the surface viscosity is $5 \pm 2 \times 10^{-6}$ sp. This value is only slightly larger than that found for SOPC bilayers at room temperature (Dimova et al., 1999a) and about the same as that found for egg phosphatidylcholine, using the filament-pulling technique (Waugh, 1982a,b). While macroscopic techniques give membrane viscosities on the order of a few 10^{-6} sp, measurements based on diffusion of molecular probes and Saffman's theory (Saffman, 1976; Hughes et al., 1981) give smaller values of $\sim 10^{-7}$ sp (see, e.g., Vaz et al., 1984; Merkel et al., 1989). We will comment on this point in section V.1.

Near the transition, η_s increased by more than two decades. We tentatively fitted a power law to the data,

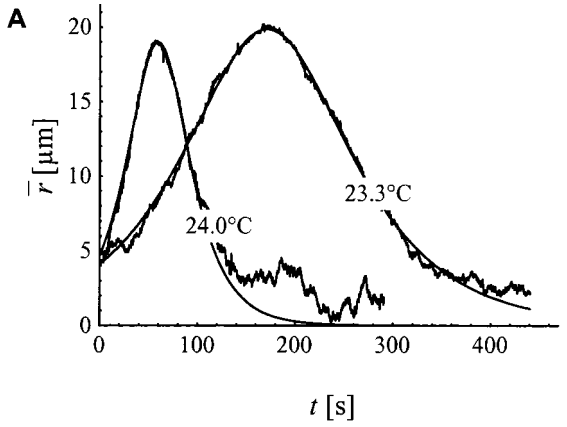

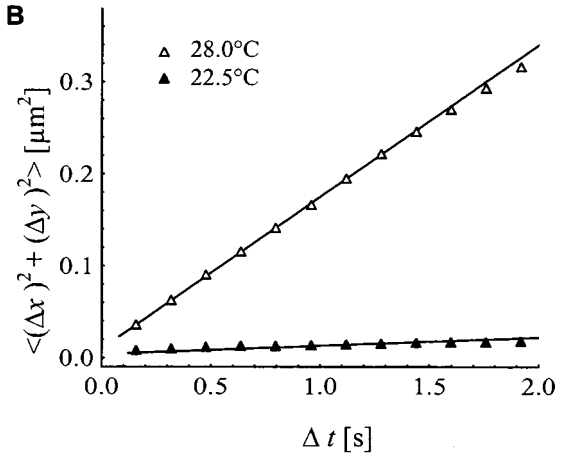

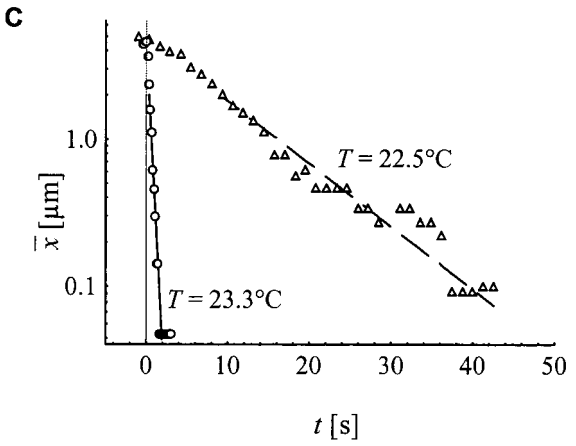

FIGURE 7 (*A*) Sedimentation particle trajectories, $\bar{r}(t)$, recorded with one bead-vesicle system (a = 3.2 μm, R = 21 μm) at two different temperatures. The fits are performed according to Eq. 5. (*B*) Brownian diffusion: calculated mean squared displacements (MSD) of the trajectories of a latex bead (a = 3.2 μm) near the bottom of a vesicle (R = 21 μm) for two different temperatures. Note: As established by computer simulations, MSD plots are affected by detection noise causing an offset: MSD = $4D\,dt + C_{noise}$. For corrected analysis, slopes (= $4D$) were obtained from line fits that cover the time regime from points 1 (≅ 1/6 s) to 4 (≅ 4/6 s), as illustrated with solid lines. (*C*) Optical trapping kinetics: displacements (logarithmic scale) of a latex bead (a = 3.2 μm, R = 21 μm), after switching on the optical trap at t = 0. Straight lines are fits according to Eq. 7 for the region $\bar{x} < 0.6a$.

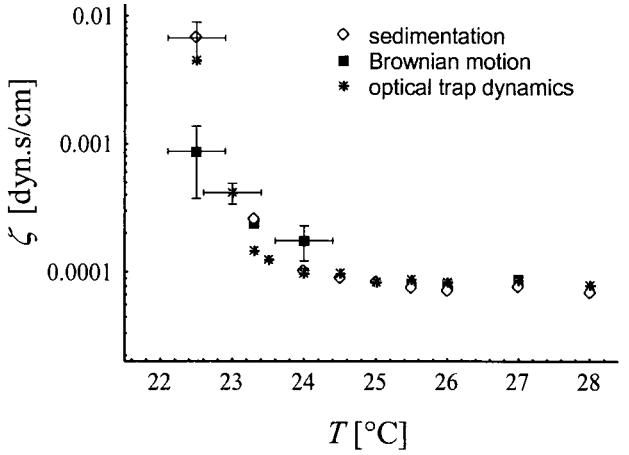

FIGURE 8 Thermal behavior of the drag coefficient of a particle bound to a vesicle membrane in the fluid phase. The graph gathers the data obtained from sedimentation-, diffusion-, and optical trap-driven motion with the same particle-vesicle system (a = 3.2 μm, R = 21 μm). Data were obtained with a primitive experimental cell (a generation before the one in Fig. 1), where the temperature was controlled within ±0.4°C.

$\eta_s \propto |T - T_m|^w$, but because of the data scatter, different sets of the three adjustable parameters (T_m, w, and the proportionality factor) were found to be equally acceptable. We restrained the choice by putting T_m = 23.4°C, which is approximately the temperature at which the membrane elastic response (approaching from $T < T_m$) vanishes, within experimental error. We thus found $\eta_s \cong 25 \times 10^{-6}|T - 23.4|^{-1.4}$ sp; this is the solid line in Fig. 9.

Not all of the particle-vesicle systems investigated behaved in the same way. In some cases, the divergence of ζ (or η_s) was less gradual than that in Fig. 9, i.e., η_s was greatly increased only very close to T_m. However, the vesicles in these cases were probably multilamellar. Indeed, these membranes were anomalously dark in the phase-contrast images. This is an indication that pretransitional phenomena show up far from T_m (a few degrees apart) only with unilamellar membranes (Jutila and Kinnunen, 1997; Bagatolli and Gratton, 1999).

IV.2. Gel-phase elastic response

The temperature dependence of the membrane stiffness in terms of the elastic spring constant, k_M, obtained from static elastic experiments is given in Fig. 10. Different sets of symbols correspond to different temperature scans. Filled and empty symbols refer to two individual two-particle-one-vesicle systems. The solid curve is a fit function (least-

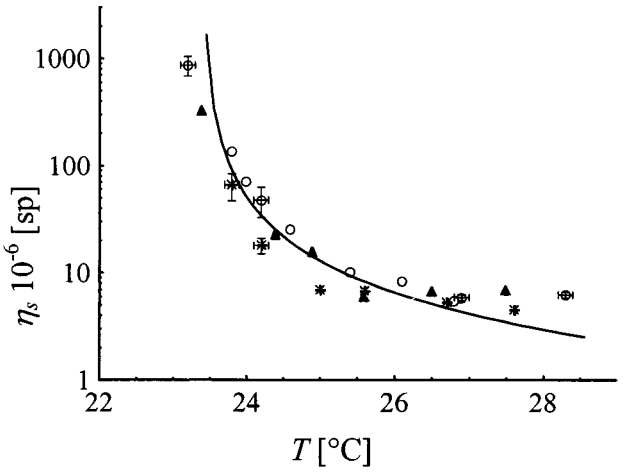

FIGURE 9 Temperature dependence of the shear surface viscosity, η_s, obtained from sedimentation experimental data for three systems: $a = 2.64$ μm, $R = 30.4$ μm, $d = -0.8$ (▲); $a = 2.7$ μm, $R = 46.4$ μm, $d = -0.9$ (○); $a = 2.72$ μm, $R = 30.5$ μm, $d = 0.1$ (*). The solid curve shows the fit by: $\eta_s = 25 \times 10^{-6}|T - 23.4|^{-1.4}$ sp.

square minimization) to the whole set of data: $k_M \cong 2.4 \times 10^{-4}\ |T - 23.4|^{1.5}$ dyn/cm. For lower temperatures (i.e., stiffer membranes) the experimental error increases because the optical trap-induced displacements (x_f and x_m; see Fig. 5) approach the pixel resolution of the camera. When the lipid enters the fluid L_α phase, the membrane looses its elastic properties and $k_M = 0$ (within the experimental accuracy). The continuous decrease in the effective stiffness as T_m is approached is an indication of a continuous gel-fluid phase transition.

A very important experimental detail to note, as we will see further, is the penetration depth of the latex beads, d. In the experiments reported here, particles are protruding predominantly on one side of the vesicle wall, $d \cong 0.8a$. For one system with $d \cong -0.8a$ (i.e., the particle centers were external to the vesicle surface; data not shown), k_M does not distinctly differ.

Finally, following the procedure described in section III.3.2, we studied the membrane relaxation response in terms of recorded interparticle distance (l) versus time (Fig. 11). First we induce a displacement of the bead held by the mobile trap. Then the particle is released, and it slowly relaxes toward its initial position. A simple exponential function (*solid line*) described by Eq. 7 adequately fits the relaxation branch of the curve. The characteristic time for membrane relaxation in this example is $\tau_r = 5$ s at $T = 19$°C.

Not all of the recorded particles relaxed according to a single exponential and returned exactly to their initial positions. In many other examples, we noticed that the particles' final positions differed from the original ones (mainly for the particle in the mobile trap), beyond experimental uncertainty, and that the relaxations, though still monotonic, were not single exponentials. In these situations, we estimated a half-time for relaxation as the point where the induced displacement dropped to half of its maximum value; the average half-time was ~7 s at all temperatures. Thus there was no acceleration or a reduction of the relaxation kinetics when the temperature was increased toward T_m. Why beads do not return to their initial positions is not obvious from the observation. As we explained in section II.1, the vesicles are connected to the cluster by contact points or contact zones. If the vesicle were free, $e - x_m$ and x_f would be equal, from

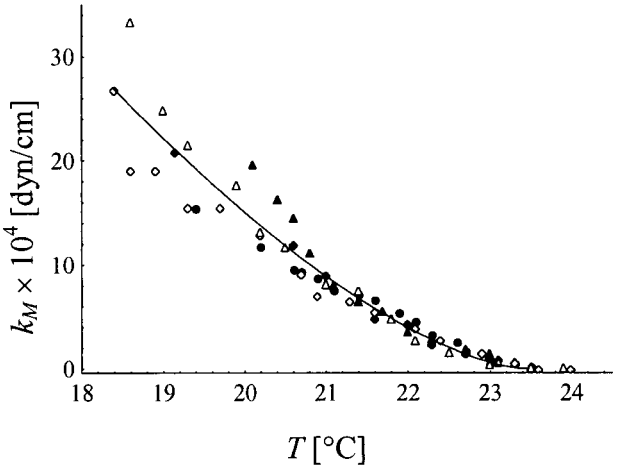

FIGURE 10 The measured membrane effective stiffness, k_M, plotted as a function of the temperature. The different sets of symbols correspond to different temperature scans. Filled and empty symbols correspond to two individual particle-vesicle systems; for all particles $a \approx 5.3$ μm, $d \cong -0.8a$. The solid curve shows the fit by $k_M = 2.4 \times 10^{-4}|T - 23.4|^{1.5}$ dyn/cm.

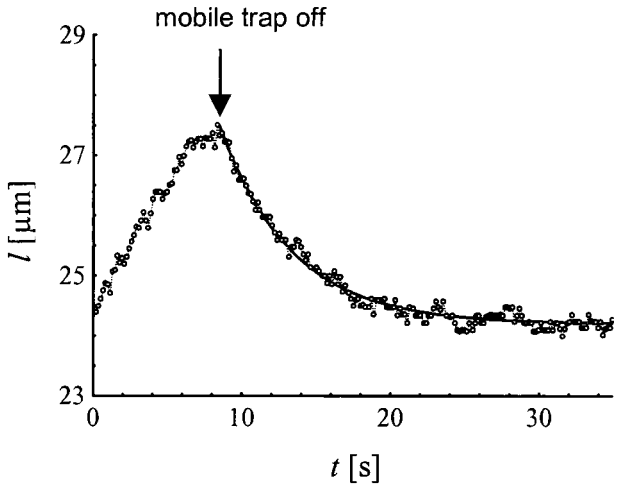

FIGURE 11 A dynamic elasticity experiment performed at $T = 19$°C. The points represent the measured interparticle distance, l, and the solid curve is an exponential fit following Eq. 11 ($\tau_r = 5$ s) to the relaxation branch of the trace.

symmetry. The fact that x_f in general is definitely smaller than $e - x_m$ is due to the above-mentioned contacts, because they hinder the overall rotation of the vesicle. It is possible that the forces exerted on the beads by the laser beams make the vesicle move slightly, precluding full reversibility.

In an individual case of large bead penetration ($d \rightarrow -1$) the particle could be repositioned to a relatively larger distance ($> a$). The average relaxation time for this particular system was about four times longer than the rest. The effect may be ascribed to eventual connection of the bead to the vesicle membrane in the form of a tether and not a definite contact line.

V. DISCUSSION

V.1. Fluid phase viscosity

A simple viscous fluid would have a constant viscosity. If the fluid is viscoelastic, η_s is defined as a complex number depending on the frequency. In the time domain, the friction would not be defined as a constant but as a time-dependent response (see, for instance, Berne and Pecora, 1976). As we explained, we analyzed our data under the assumption that ζ was a constant. If this was not so, the recorded trajectories would show systematic deviations from the equations set out in section III.1. In fact, experiments are consistent with the assumption of ζ = constant, within experimental error. We may translate this statement in terms of frequency: in Fig. 7 *C*, the trapping kinetics at 23.3°C were recorded from ~0.1 to 1 s and were found to be exponential in this range. In Fig. 7 *A* the sedimentation motion at the same temperature was well fitted by Eq. 5 in a 200-s time interval, indicating that no viscoelastic behavior was detected in the 0.01–10-Hz interval.

The drastic increase in η_s can be interpreted in terms of pretransitional structure fluctuations in the membrane. The so-called fluid (or liquid crystalline) state is only defined as an average, so that a snapshot of the film at the molecular level would in fact reveal a nonhomogeneous structure, essentially a mixture of fluid-like and gel-like domains. While such a snapshot is not feasible, at this juncture, from experiments on real systems, computer simulations clearly show this behavior (Ipsen et al., 1990; Pedersen et al., 1996; Hønger et al., 1996; Jørgensen et al., 1996). A similar description was also proposed from real experiments with fluorescent probes: different quenchers partitioning in either gel or fluid phases were used, and results for the sample fluorescence intensity were interpreted in terms of lipid microdomain formation (Pedersen et al., 1996). Gel-like domains have finite sizes and lifetimes (these can be represented by a correlation length, ξ, and a correlation time, τ), which increase near T_m. If the transition is continuous, ξ and τ diverge to infinity at T_m, which means practically that domains reach a size on the order of the vesicle size.

Qualitatively, the increase in ξ and τ results in a macroscopically more viscous phase, and this is detected by the polystyrene particles. Molecular probes do detect the proximity of the transition too, as their Brownian motion is slowed down when the temperature is decreased (for a review see Clegg and Vaz, 1985). But their size is much smaller than ξ near T_m (the gel-like domains are largely supramolecular); consequently, the membrane viscosity is hard to define. Because the latex beads are macroscopic ($a \gg \xi$, except perhaps exceedingly close to T_m), they do experience the large scale viscosity, η_s.

At high temperature ($T \gg T_m$), the domain size should decrease substantially. In this limit, one might expect a convergence of viscosities found with macroscopic techniques ($\eta_{s,\,macro}$) and those found with molecular probes ($\eta_{s,\,mol}$). Practically, the reduced temperature ($T - T_m$) that puts the bilayer in the high-temperature regime is difficult to define. For $T - T_m$ on the order of 10°C, $\eta_{s,\,mol}$ values are in general smaller than $\eta_{s,\,macro}$ values, as we mentioned in section IV.1. While we have no concrete explanation for this difference, we may speculate that the membrane structure is still not that of a simple liquid, even several degrees above T_m. In other words, the fact that $\eta_{s,\,mol} \ll \eta_{s,\,macro}$ may indicate that lipid bilayers in the fluid phase are not self-similar on the molecular scale.

By analogy with percolation phenomena theories, one might conjecture that η_s varies as $\langle \bar{R}^2 \rangle$, the average value of the gel domain size squared (Jouhier et al., 1983). Our data would then suggest that $\langle \bar{R}^2 \rangle$ varies as $|T - T_m|^{-1.4}$, approximately. This conjecture can be tested, as $\langle \bar{R}^2 \rangle$ can be readily computed from numerical simulations.

V.2. Gel-phase elasticity

The goal of this section is to relate the effective membrane stiffness, k_M, to the basic parameters characterizing the membrane elasticity: the compressibility/expansion modulus, K_a, the shear modulus, μ, and the curvature modulus, k_C. We start the discussion by defining the geometry of the two-bead-membrane system. Fig. 12 *A* represents the conditions of our experiments in the gel phase: the two beads were located very much toward the vesicle interior ($d \cong -0.8$), which means that their centers were definitely outside of the membrane plane (the membrane is approximately flat on the scale of the interparticle distance). We recall that the optical trap forces act on the particles through their centers.

A second important feature of the system is what we briefly mentioned as "contact-line pinning." In practice this means that the lipid in contact with the particle is locked on the particle surface. Thus the beads cannot glide along the membrane. Note that if they could glide on the gelled surface, there would be no elastic restoring force at equilibrium.

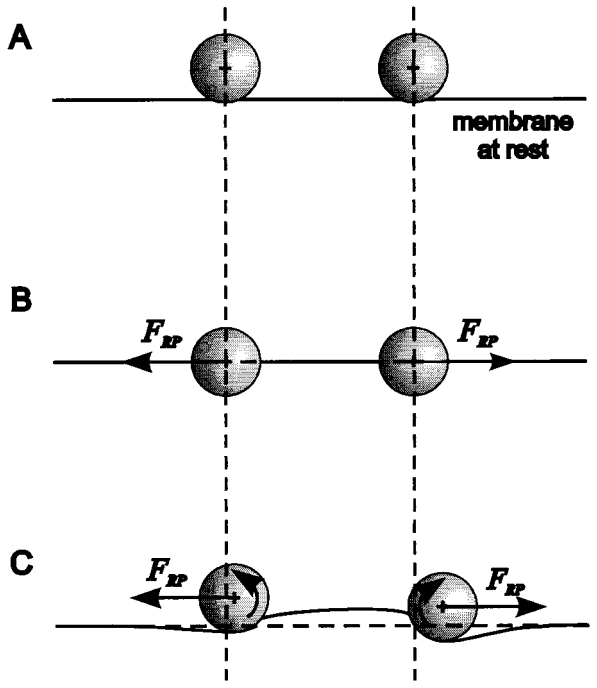

FIGURE 12 Scheme of the two-particle flat membrane geometry. (*A*) Unperturbed state with particles penetrating a small amount. (*B*) Particles with penetration $d = 0$. (*C*) A tentative representation of the out-of-plane deformation induced by the radiation pressure forces.

We now want to guess the type of deformation that is produced by the radiation pressure forces acting on the particles. If the membrane was restrained to stay flat, the deformation would be a mixture of in-plane compression/expansion and shear. Such a situation would be realized in the configuration sketched in Fig. 12 *B*; there the bead centers are located in the membrane plane ($d = 0$), and so are the radiation pressure forces. In this geometry, increasing the interparticle distance essentially amounts to elongating the membrane between the two beads. An approximate solution of this problem can be worked out from the available literature on the elasticity of 2-D systems (Muskhelishvili, 1963). One finds that k_M is approximately proportional to the membrane shear modulus, $k_M \cong 8\pi\mu/\ln(l_0/a)$, provided that $\mu \ll K_a$, meaning that k_M is on the order of μ. If we apply this equation to our data, we arrive at extremely small values of μ, e.g., $\mu \approx 10^{-3}$ dyn/cm at 20°C (Dimova et al., 1999b).

This result calls for three remarks:

1. Such a small value of μ is not possible with a 2-D system in the crystalline state. Indeed, a 2-D crystal should melt at a temperature on the order of $\mu s^2/k_B$ (Nelson and Halperin, 1979), where s is a molecular length (~1 nm), giving an unreasonable value for T_m (~ 0.1 K).

2. Gel phases may be viewed as mixtures of fluid and ordered regions (Rappolt and Rapp, 1996). A naive model supposes that we have a fluid membrane plus a 2-D network of an elastic material (e.g., the spectrin network of the erythrocyte membrane, or polymer -decorated membranes for which a similar value of μ was measured; see Helfer, 1999). In this case, we estimate μ to be on the order of $\mu_{el}\phi$, where μ_{el} is the shear modulus of the elastic material and ϕ is the surface area fraction covered by this material. If we apply this model to our problem, we arrive at a value for ϕ on the order of 0.001, at most. If the elastic fraction of the gel phase were so small, this would have been noticed in x-ray spectra. Moreover, the elastic part of the gel phase has to be "percolating," otherwise the system could not be elastic on a macroscopic scale. If $\phi \leq 0.001$, the elastic part must be extremely filamentous, which is not detected in x-ray spectra.

3. Membranes are not exactly 2-D systems. Out-of-plane fluctuations make them actually 3-D systems, which can still be described as 2-D, but with renormalized Lamé and curvature constants. One may conjecture that lipid membrane gel phases are not crystals (in the sense of long-range positional order), but hexatics with a small finite value of μ (Nelson and Peliti, 1987). To our knowledge, this conjecture is not supported or ruled out by x-ray observations, i.e., there is no definite evidence that the order in gel phases is hexatic rather than crystalline (see Smith et al., 1988).

We instead propose a simple explanation, based on the sketch shown in Fig. 12, that the out-of-plane radiation pressure forces produce an out-of-plane deformation of the membrane. In principle, such a deformation requires both a curvature energy, E_C, and a dilatation energy, E_a. The origin of the dilatation term is apparent if we assume an initially perfectly spherical vesicle and require that the volume inside it be conserved. Increasing the interparticle distance by about a then costs an energy E_a on the order of $K_a\, a^2$, at least, which in our system is enormous, $\sim 10^8\ k_BT$. The optical trapping energy is much too small to produce such a deformation. However, the dilatation energy is reduced and even drops to zero if the vesicle initially has excess area arising from a slightly nonspherical shape (for an isolated vesicle). In this situation, the membrane tension at rest is negligible, and we assume this for our experimental conditions, because particles can be moved by the radiation pressure forces. (A second but indirect argument comes from the reproducibility of the dynamometry experiment in repeated cooling-heating cycles. Initially, the vesicles prepared in the L_α phase are quasispherical and therefore have little excess area. Cooling to the gel phase shrinks the surface considerably (by ~20%; see Needham and Evans, 1988), and the volume inside cannot be conserved (the membrane cannot sustain the resulting stress without rupture). Reheating the sample beyond T_m produces highly nonspherical vesicles (see also Bagatolli and Gratton, 1999), because they now have very large excess areas. After the sample is again cooled down to the gel state, the dynamometry experiment is repeated, as we explained. Because the measured values of k_M are reproduced, we conclude that

the initial excess area does not influence the membrane effective stiffness. This is a strong indication that the membrane tension of the gelled vesicles is relaxed, whatever the initial (in L_α phase) vesicle excess area might have been. A third argument is that the gelled vesicles that we experimented on were still touching neighbors through easily visible contact points or zones, and were not perfectly spherical.)

Having dropped the dilatation term, we are now left only with the curvature energy. Following the arguments given in the Appendix, we expect the resulting effective stiffness to be on the order of k_C/a^2. In the absence of an appropriate theory, we tested this conjecture by simple experiments on a few macroscopic sheets (see Appendix) made of different materials. This analog simulation showed that

$$k_M \cong Ck_C/a^2, \tag{12}$$

where $C \cong 60$. The result is approximate (the empirical formula holds only within a factor of 2 among the examples studied) but allows us to roughly deduce the value of the DMPC membrane curvature modulus in the gel phase.

Fig. 13 presents the temperature dependence of the curvature constant in k_BT units (*empty circles*) deduced from the effective spring constant data below T_m according to Eq. 12. The right part of the figure ($T > T_m$) presents values of k_C (*diamonds*) extracted from the analysis of thermal fluctuations of DMPC vesicles in the fluid phase and taken from Méléard et al. (1997). A large number of methods have been developed to measure the membrane bending stiffness (see refs. in Méléard et al., 1997; Beblik et al., 1985; Zhelev et al., 1994), but we do not know of any direct measurement of the bending modulus of lipid bilayers in the gel phase.

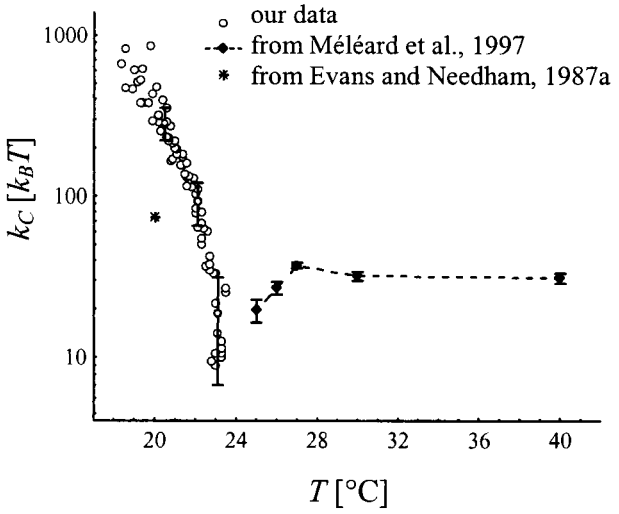

FIGURE 13 Thermal behavior of the gel-state membrane curvature modulus. ○, The values of k_C were deduced from those of k_M according to Eq. 12. ◆, Values of k_C for fluid DMPC vesicles, taken from Méléard et al. (1997). *, Single result on k_C at $T = 20$°C, taken from Evans and Needham (1987a).

k_C can be deduced from the expansion modulus, K_a, if the bilayer is regarded as being made of two parallel elastic sheets of lateral compressibility $K_a/2$ and separated by a distance h; this gives $k_C = K_a h^2/4$ (Heimburg, 1998). According to another model the measured surface compressibility is interpreted as an extension of the ripples in the P'_β phase due to bending deflections of individual pleats of the corrugated surface; in this model $k_C \cong K_a\bar{h}^2/8$, where $\bar{h}$ is the peak-to-peak amplitude of the surface ripple (Evans and Needham, 1987a,b). Different experimental methods are sensitive to variations in the surface area of membranes and can be exploited to yield estimates of k_C. We have already mentioned the micropipette technique, from which a direct measurement of K_a can be performed (Needham and Evans, 1988; Needham and Zhelev, 1996) for vesicles in gel phase. The single result extracted from the compressibility modulus for the bending stiffness of the P'_β phase at $T = 20$°C (3×10^{-12} dyn.cm) (Evans and Needham, 1987a) is indicated in Fig. 13 (*asterisk*) and is not negligibly lower than our results.

Calorimetry and characteristics of sound propagation in vesicle suspensions yield values of K_a as well and can be used to deduce the behavior of k_C (Heimburg, 1998; Mitaku et al., 1978). Recently, Heimburg (1998) interpreted data on the heat capacity of a suspension of DPPC (1,2-dipalmitoyl-*sn*-glycero-3-phosphocholine) vesicles in this way and deduced the evolution of k_C on both sides of T_m. This study was performed with extruded and with sonicated unilamellar vesicles and with multilamellar vesicles and showed strong decreases in k_C near T_m. The anomaly in k_C was found to be more pronounced with multilamellar vesicles. Interestingly, Heimburg's result (Heimburg, 1998) for extruded large unilamellar vesicles is quantitatively close to ours below T_m (in Heimburg, 1998, the predictions of k_C are presented as a function of the reduced temperature, $T - T_m$, which allows for the data comparison). Furthermore, it confirms the measurements of Méléard et al. (1997), who reported a decrease in k_C when the temperature is decreased to T_m. The macroscopic enthalpy fluctuations near T_m are interpreted as being due to a drop in K_a, which in turn is expected to produce a drop in k_C. Qualitatively similar results were arrived at by Mitaku et al. (1978), who studied the sound propagation velocities and attenuation in DMPC and DPPC vesicle suspensions. Both quantities showed anomalies near T_m that were more pronounced with multilamellar membranes.

Other techniques are sensitive to geometrical properties of the system, which is either a giant vesicle or a lamellar (smectic) phase of lipid membranes. Experiments with DMPC vesicles in the fluid state showed that the amplitude of the shape fluctuations increases near T_m, which can be taken as direct proof that k_C decreases in this region (Fernandes-Puente et al., 1994). For the same reason, mem-

branes constituting a lamellar phase become more wrinkled in the vicinity of T_m, and this has the consequence of increasing the average distance between lamellae (Hønger et al., 1994).

To summarize, the results from different techniques all lead to a view that k_C decreases considerably near T_m on both sides of the transition. Basically, the membrane becomes more flexible because each monolayer becomes more compressible. It is then easy to locally bend the membrane by decreasing the density of the outside leaflet and increasing that of the inside one. In the recent general theory by Hansen et al. (1998), each monolayer is modeled as a 2-D fluid close to a critical point (the 2-D analog of the liquid vapor critical point), which is the source of the diverging compressibility, and coupling of the leaflet densities is taken into account. The theory of Ipsen et al. (1990) makes a prediction for the curvature modulus, which we may summarize as $k_C \approx |T - T_m|$. Note that the value of the critical exponent found from our data turns out to be larger than 1 ($\sim$1.5), which means a faster decrease than theory predicts.

Because no dynamic theory is available (the static theory is already very complex), no accurate prediction can be made for the relaxation time of the interparticle distance (τ_r) in our experimental scheme. Keeping in mind that the particles excite deformations on a scale on the order of a, we may suppose that $\tau_r \propto \eta a^3/k_C$ (Milner and Safran, 1987), where η is the water viscosity. Because k_C vanishes near T_m, a critical slowing down of the relaxation should be observed. Despite the scatter, our τ_r data do not reveal this tendency.

At this stage, we conjecture that friction inside the membrane (the bilayer viscous modes in general; see Seifert and Langer, 1993), rather than that of water, is the main source of dissipation in the process and that it decreases in about the same way as k_C near T_m.

VI. CONCLUSIONS AND PROSPECTS

In this work, we used micron-sized latex beads to mechanically probe the viscous and elastic properties of giant vesicle membranes made of DMPC. When the temperature is above the main phase transition ($T_m \cong 23.6$°C; see Koynova and Caffrey, 1998), the DMPC is fluid, but its shear viscosity increases considerably near T_m. As far as we know, this work is the first presenting a quantitative study of the DMPC membrane hydrodynamic shear viscosity, η_s, and its critical behavior near the fluid-to-gel transition of the lipid membrane. By "hydrodynamic" we mean a viscosity defined on a scale much larger than structural details of the membrane, particularly the correlation length of gel-like structural fluctuations in the fluid phase. The drastic increase in η_s near T_m may be thought of as being due to renormalization of the membrane viscosity by these fluctuations. The measured η_s should be regarded as being in the zero frequency limit as well. We did not find any indication of a viscoelastic behavior up to a few Hz.

In the gel phase ($T < T_m$), we probed the elasticity of the DMPC membrane by means of two latex particles, which have almost a point contact with the membrane. We could modify the distance between the particle centers by using radiation pressure forces of the laser beams. The membrane produces an elastic force to oppose this deformation, which is characterized by an effective membrane stiffness, k_M. Near T_m, we found a marked decrease in k_M. No slowing of the system relaxation dynamics was observed. We interpreted the membrane response as mainly being due to curvature elasticity (k_C modulus). Following this interpretation, the experiments with the two latex beads allowed us to directly feel and measure the curvature modulus of a solidified membrane and to characterize its pretransitional behavior. Our results are in line with others from the literature, which were indirectly related to curvature elasticity.

Our interpretation of k_M in terms of the curvature elasticity is still tentative and might be improved by future developments, in both experiments and theory. For instance, our analysis predicts that k_M should depend strongly on the particle penetration. Up to now we have not prepared a system with two particles whose centers are located in the membrane plane ($d \cong 0$), but this should be feasible. Such a system should be almost nondeformable by the radiation pressure forces ($k_M \to 0$). Theoretically, there is a need for a general analysis of the two spherical particle-membrane system, taking into account out-of-plane deformations. This would be a very useful tool for interpreting optical or magnetic dynamometry experiments based on this geometry.

APPENDIX: EXPERIMENTS WITH MACROSCOPIC SHEETS

In the absence of external forces the equation of the deformation of a plate is simply $\Delta^2 u = 0$, where u denotes the displacement of a point from the surface. No intrinsic length is introduced. For trivial boundary conditions ($u = 0$ far from the perturbation) the only characteristic length of the problem is imposed by the source of the deformation. We thus assume that the range of the induced perturbation is on the order of the particle size a. The bending energy is $E_C \propto (1/2)k_C(u/a^2)^2a^2 \cong (1/2)k_C$. On the other hand, the energy corresponding to the measured effective stiffness is $E_C \propto (1/2)k_M a^2$. Therefore we expect $k_M \cong Ck_C/a^2$, where C is a constant. To test this conjecture, we performed simple measurements on several macroscopic sheets. We used essentially "nonshearable" ($\mu = \infty$) materials: polyethylene, polycarbonate, stainless steel. The experimental set-up is sketched in Fig. 14. To measure k_M, we model the particle-vesicle system with a ball attached (by a point contact) to a flat sheet (Fig. 14 *A*) or to the wall of a cylinder (Fig. 14 *B*). Of course, modeling the vesicle surface with a flat sheet or cylinder amounts to omitting the condition of conservation of the vesicle volume. A lever attached to the ball is loaded, and the corresponding deviation is measured (the deviation is rescaled to correspond to a force applied to the center of the ball and not at the tip of the lever). The sheet response is linear within the region of deformation that is less than or equal to $0.15a_{ball}$ (a_{ball} is the ball radius). k_C was measured independently: the sheet was clamped horizontally along an edge and left hanging under its own weight. The profile of the sheet perpendicular to the

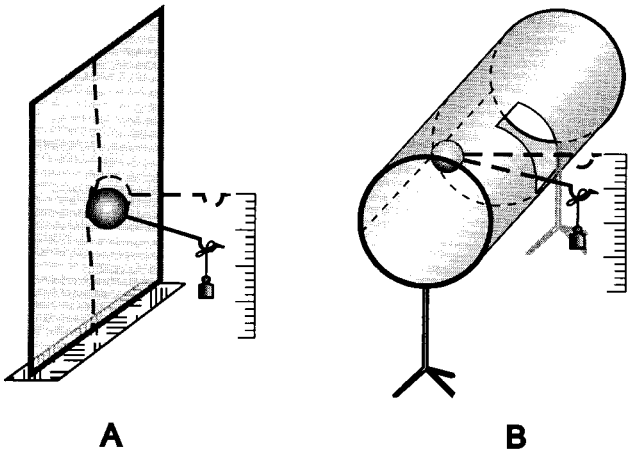

FIGURE 14 Sketches of model experiments on macroscopic sheets. (*A*) Flat sheet model. (*B*) Cylindrical geometry.

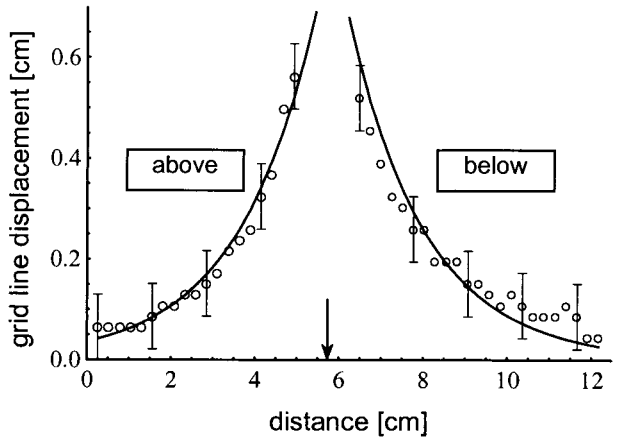

FIGURE 16 Out-of-plane deformation of a polycarbonate sheet in the geometry of Fig. 14 *A*. The ball position is indicated by the arrow.

clamped edge was measured and fitted by the theoretical profile (Landau and Lifshitz, 1986). Results for the effective spring constant and the bending elasticity modulus from the cylindrical model (Fig. 14 B) agree fairly well with the linear relation $k_M \propto k_C/a_{ball}^2$ (see Fig. 15). The intercept on the ordinate provides the coefficient of proportionality $C_{cyl} \cong 24.5$ (data are plotted on a double logarithmic scale). To account for curvature effects from vesicle sphericity we introduced an approximate correction factor of $\sim$2.5 (or $C \cong 60$), corresponding to the difference between the responses detected from the plane and cylindrical models.

We studied the deformation by using a polycarbonate sheet in the flat configuration (Fig. 14 *A*). A line grid (*horizontal lines*) was optically projected onto the sheet, which acted as a mirror. With a video camera, we recorded the image of the grid, first when the sheet was at rest (no load) and then when the ball was loaded. The sheet deformation due to loading produced an easily visible deformation of the lines in the image of the grid. The displacement of the grid lines along the vertical section across the particle center is displayed in Fig. 16. An exponential can be fitted to both branches, above (*left graph*) and below (*right graph*) the particle. We find a decay length $L \cong 1.85$ cm in this example, while $a_{ball} = 1.51$ cm. This result supports our intuition that L should be on the order of a_{ball}. This rough analog simulation yields results in agreement with our conjecture that k_M is proportional to k_C/a^2.

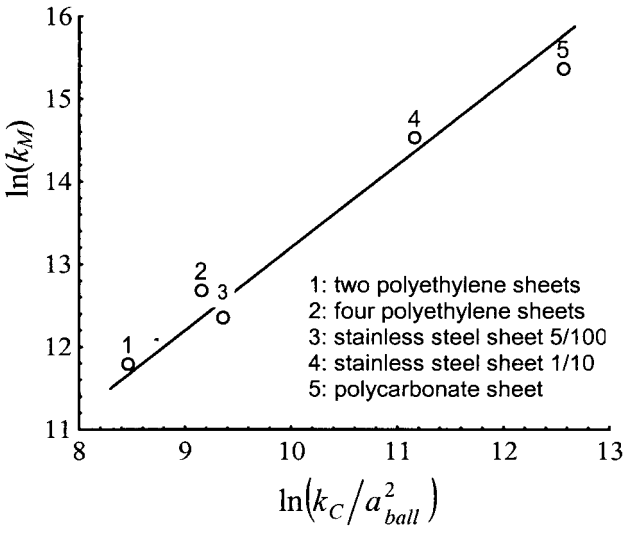

FIGURE 15 Test of the $k_M = Ck_C/a^2$ relation. Measurements were performed on sheets of different materials, as indicated.

We thank K. Jacobson for his critical reading of the manuscript and his help with the writing style; M. Angelova, P. Méléard, P. Martinoty, and L. Salomé for their interest and helpful comments; and G. Gréhan for the kind provision of the GLMT program.

This work was carried out in the framework of the "Laboratoire Franco-Bulgare" (LFB), a joint structure between the Centre National de la Recherche Scientifique (CNRS), the Bulgarian Academy of Sciences, and Sofia University. One of us (RD) is grateful to the French government for a 15-month grant and to the LFB for a 5-month grant.

REFERENCES

Angelova, M. I., and D. S. Dimitrov. 1986. Liposome electroformation. *Faraday Discuss. Chem. Soc.* 81:303–311.

Angelova, M. I., and B. Pouligny. 1993. Trapping and levitation of a dielectric sphere with off-centered Gaussian beams. I. Experimental. *Pure Appl. Opt. A.* 2:261–276.

Angelova, M. I., S. Soléau, P. Méléard, J. F. Faucon, and P. Bothorel. 1992. Preparation of giant vesicles by external AC electric fields. Kinetics and applications. *Prog. Colloid Polym.* 89:127–131.

Ashkin, A. 1997. Optical trapping and manipulation of neutral particles using lasers. *Proc. Natl. Acad. Sci. USA.* 94:4853–4860.

Ashkin, A., J. M. Dziedzic, J. E. Bjorkholm, and S. Chu. 1986. Observation of a single-beam gradient force optical trap for dielectric particles. *Opt. Lett.* 11:288–290.

Bagatolli, L. A., and E. Gratton. 1999. Two-photon fluorescence microscopy observations of shape changes at the phase transition in phospholipid giant unilamellar vesicles. *Biophys. J.* 77:2090–2101.

Bar-Ziv, R., R. Menes, E. Moses, and S. A. Safran. 1995. Local unbinding of pinched membranes. *Phys. Rev. Lett.* 75:3356–3359.

Bausch, A. R., W. Möller, and E. Sackmann. 1999. Measurement of local viscoelasticity and forces in living cells by magnetic tweezers. *Biophys. J.* 76:573–579.

Bausch, A. R., F. Ziemann, A. A. Boulbitch, K. Jacobson, and E. Sackmann. 1998. Local measurement of viscoelastic parameters of adherent cell surfaces by magnetic bead micrometry. *Biophys. J.* 75:2038–2049.

Beblik, G., R.-M. Servuss, and W. Helfrich. 1985. Bilayer bending rigidity of some synthetic lecithins. *J. Physique*. 46:1773–1778.

Berne, B. J., and R. Pecora. 1976. Dynamic Light Scattering. John Wiley and Sons, New York.

Boulbitch, A. A. 1999. Strain of a biomembrane caused by a local tangential force: application to magnetic tweezers measurements. *Phys. Rev. E.* 59:3402–3407.

Brady, G. W., and D. B. Fein. 1977. An analysis of the x-ray interchain peak profile in dipalmitoylglycerolphosphocholine. *Biochim. Biophys. Acta*. 464:249–259.

Bronkhorst, P. J. H., G. J. Streekstra, J. Grimbergen, E. J. Nijhof, J. J. Sixma, and G. J. Brakenhoff. 1995. A new method to study shape recovery of red blood cells using multiple optical trapping. *Biophys. J.* 69:1666–1673.

Clegg, R. M., and W. L. C. Vaz. 1985. Translational diffusion of proteins and lipids in artificial lipid bilayer membranes. A comparison of experiment with theory. *In* Progress in Protein-Lipid Interactions. A. Watts and J. J. H. H. M. De Pont, editors. Elsevier, Amsterdam. 173–229.

Danov, K., R. Aust, F. Durst, and U. Lange. 1995. Influence of the surface viscosity on the hydrodynamic resistance and the surface diffusivity of a large Brownian particle. *J. Colloid Interface Sci.* 175:36–45.

Davis, J. H. 1979. Deuterium magnetic resonance study of the gel and liquid crystalline phases of dipalmitoyl phosphatidylcholine. *Biophys. J.* 27:339–358.

Derzko, Z., and K. Jacobson. 1980. Comparative lateral diffusion of fluorescent lipid analogues in phospholipid multibilayers. *Biochemistry*. 19:6050–6057.

Dietrich, C., M. I. Angelova, and B. Pouligny. 1997. Adhesion of latex spheres to giant phospholipid vesicles: statics and dynamics. *J. Phys. II France*. 7:1651–1682.

Dimova, R., C. Dietrich, A. Hadjiisky, K. Danov, and B. Pouligny. 1999a. Falling ball viscosimetry of giant vesicle membrane: finite-size effects. *Eur. Phys. J. B.* 12:589–598.

Dimova, R., C. Dietrich, and B. Pouligny. 1999b. Motion of particles attached to giant lipid vesicles: falling-ball viscosimetry and elasticity measurements on lipid membranes. *In* Giant Vesicles. P. Walde and P. Luisi, editors. John Wiley and Sons, New York. 221.

Evans, E., and R. Kwok. 1982. Mechanical calorimetry of large dimyristoylphosphatidylcholine vesicles in the phase transition region. *Biochemistry*. 21:4874–4879.

Evans, E., and D. Needham. 1987a. Physical properties of surfactant bilayer membranes: thermal transitions, elasticity, rigidity, cohesion, and colloidal interactions. *J. Phys. Chem.* 91:4219–4228.

Evans, E., and D. Needham. 1987b. Surface density transitions, surface elasticity and rigidity, and rupture strength of lipid bilayer membranes. *In* Physics of Amphiphilic Layers. J. Meunier, D. Langevin, and N. Boccara, editors. Springer-Verlag, Berlin and Heidelberg. 38–57.

Fernandes-Puente, L., I. Bivas, M. D. Mitov, and P. Méléard. 1994. Temperature and chain-length effects on bending elasticity of phosphatidylcholine bilayers. *Europhys. Lett.* 28:181–186.

Gouesbet, G., B. Maheu, and G. Gréhan. 1988. Light scattering from a sphere arbitrarily located in a Gaussian beam, using a Bromwich formulation. *J. Opt. Soc. Am. A.* 5:1427–1443.

Granek, G., P. Nelson, T. Powers, and U. Seifert. 1995. Dynamics of Rayleigh-like instability induced by laser tweezers in tubular vesicles of self-assembled membranes. *J. Phys. II France.* 5:1348–1370.

Hansen, P. L., L. Miao, and J. H. Ipsen. 1998. Fluid, lipid bilayers: intermonolayer coupling and its thermodynamic manifestations. *Phys. Rev. E.* 58:2311–2324.

Heimburg, T. 1998. Mechanical aspects of membrane thermodynamics. Estimation of the mechanical properties of lipid membranes close to the chain melting transition from calorimetry. *Biochim. Biophys. Acta.* 1415: 147–162.

Helfer, E. Micromécanique de membranes solides artificielles. 1999. Thése de Doctorat. Université de Strasbourg.

Hénon, S., G. Lenormand, A. Richert, and F. Gallet. 1999. A new determination of the shear modulus of the human erythrocyte membrane using optical tweezers. *Biophys. J.* 76:1145–1151.

Hochmuth, R. M., K. L. Buxbaum, and E. A. Evans. 1980. Temperature dependence of the viscoelastic recovery of red cell membrane. *Biophys. J.* 29:177–182.

Hønger, T., K. Jørgensen, R. L. Biltonen, and O. G. Mouritsen. 1996. Systematic relationship between phospholipase A_2 activity and dynamic lipid bilayer microheterogeneity. *Biochemistry.* 35:9003–9006.

Hønger, T., K. Mortensen, J. H. Ipsen, R. Bauer, and O. G. Mouritsen. 1994. Anomalous swelling of multilamellar lipid bilayers in the transition region by renormalization of curvature elasticity. *Phys. Rev. Lett.* 72:3911–3914.

Hughes, B. D., B. A. Pailthorpe, and L. R. White. 1981. The translational and rotational drag on a cylinder moving in a membrane. *J. Fluid Mech.* 110:349–372.

Ipsen, J. H., K. Jorgensen, and O. G. Mouritsen. 1990. Density fluctuations in saturated bilayers increase as the acyl-chain decreases. *Biophys. J.* 58:1099–1107.

Janiak, M. J., D. M. Small, and G. G. Shipley. 1976. Nature of the thermal pretransition of synthetic phospholipids: dimyristoyl- and dipalmitoyllecitin. *Biochemistry.* 21:4575–4580.

Janiak, M. J., D. M. Small, and G. G. Shipley. 1979. Temperature and compositional dependence of the structure of hydrated dimyristoyl lecithin. *J. Biol. Chem.* 254:6068–6078.

Jørgensen, K., A. Klinger, M. Braiman, and R. L. Biltonen. 1996. Slow nonequilibrium dynamical rearrangement of the lateral structure of a lipid membrane. *J. Phys. Chem.* 100:2766–2769.

Jouhier, B., C. Allain, B. Gauthier-Manuel, and E. Guyon. 1983. The sol-gel transition. *Ann. Isr. Phys. Soc.* 5:167–185.

Jutila, A., and P. K. J. Kinnunen. 1997. Novel features of the main transition of dimyristoylphosphatidylcholine bilayers revealed by fluorescence spectroscopy. *J. Phys. Chem. B.* 101:7635–7640.

Koynova, R., and M. Caffrey. 1998. Phases and phase transitions of the phosphatidylcholines. *Biochim. Biophys. Acta.* 1376:91–145.

Landau, L. D., and E. M. Lifshitz. 1986. Theory of elasticity. *In* Course of Theoretical Physics. E. M. Lifshitz, A. M. Kosevitz, and L. P. Pitaevskii, editors. Pergamon Press, Oxford, New York, Beijing, Frankfurt, São Paulo, Sydney, Tokyo, Toronto. 38–45.

Liu, Y., D. K. Cheng, G. J. Sonec, M. W. Berns, and B. J. Tromberg. 1995. Evidence for localized cell heating induced by infrared optical tweezers. *Biophys. J.* 68:2137–2144.

MacKay, A. L. 1981. A proton NMR moment study of the gel and liquid-crystalline phases of dipalmitoyl phosphatidylcholine. *Biophys. J.* 35:301–313.

Martinot-Lagarde, G., B. Pouligny, M. I. Angelova, G. Gréhan, and G. Gouesbet. 1995. Trapping and levitation of a dielectric sphere with off-centered Gaussian beams. I. GLMT analysis. *Pure Appl. Opt.* 4:571–585.

Méléard, P., C. Gerbaud, T. Pott, L. Fernandes-Puente, I. Bivas, M. Mitov, J. Dufourcq, and P. Bothorel. 1997. Bending elasticities of model membranes: influences of temperature and sterol content. *Biophys. J.* 72:2616–2629.

Merkel, R., E. Sackmann, and E. Evans. 1989. Molecular friction and epitactic coupling between monolayers in supported bilayers. *J. Phys. France.* 50:1535–1555.

Milner, S. T., and S. A. Safran. 1987. Dynamical fluctuations of droplet microemulsions and vesicles. *Phys. Rev. A.* 36:4371–4379.

Mitaku, S., A. Ikegami, and A. Sakanishi. 1978. Ultrasonic studies of lipid bilayer. Phase transition in synthetic phosphatidylcholine liposomes. *Biophys. Chem.* 8:295–304.

Muskhelishvili, N. I. 1963. Some Basic Problems of the Mathematical Theory of Elasticity. P. Noordoff, Groningen, the Netherlands.

Needham, D., and E. Evans. 1988. Structure and mechanical properties of giant lipid (DMPC) vesicle bilayers from 20°C below to 10°C above the liquid crystal-crystalline phase transition at 24°C. *Biochemistry.* 27: 8261–8269.

Needham, D., and D. V. Zhelev. 1996. The mechanochemistry of lipid vesicles examined by micropipet manipulation techniques. *In* Vesicles. M. Rossof, editor. Marcel Dekker, New York, Basel, and Hong Kong. 373–444.

Nelson, D. R., and B. I. Halperin. 1979. Dislocation-mediated melting in two dimensions. *Phys. Rev. B.* 19:2457–2484.

Nelson, D. R., and L. Peliti. 1987. Fluctuations in membranes with crystalline and hexatic order. *J. Physique.* 48:1085–1092.

Pedersen, S., K. Jørgensen, T. R. Bækmark, and O. G. Mouritsen. 1996. Indirect evidence for lipid-domain formation in the transition region of phospholipid bilayers by two-probe fluorescence energy transfer. *Biophys. J.* 71:554–560.

Pink, D. A., T. J. Green, and D. Chapman. 1980. Raman scattering in bilayers of saturated phosphatidylcholines. Experiment and theory. *Biochemistry.* 19:349–356.

Polaert, H., G. Gréhan, and G. Gouesbet. 1998. Forces and torques exerted on a multilayered spherical particles by a focused Gaussian beam. *Opt. Commun.* 155:169–179.

Rappolt, M., and G. Rapp. 1996. Structure of the stable and metastable ripple phase of dipalmitoylphosphatidylcholine. *Eur. Biophys. J.* 24: 381–386.

Ren, K. F., G. Gréhan, and G. Gouesbet. 1994. Radiation pressure forces exerted on a particle arbitrarily located in a Gaussian beam, using the generalized Lorenz-Mie theory, and associated resonance effects. *Opt. Commun.* 108:343–354.

Saffman, P. G. 1976. Brownian motion in thin sheets of viscous fluid. *J. Fluid Mech.* 73:593–602.

Schneider, M. B., K. W. Chan, and W. W. Webb. 1983. Fast diffusion along defects and corrugations in phospholipid P'_β liquid crystals. *Biophys. J.* 43:157–165.

Seifert, U., and S. A. Langer. 1993. Viscous modes of fluid bilayer membranes. *Europhys. Lett.* 23:71–76.

Seung, H. S., and D. R. Nelson. 1988. Defects in flexible membranes with crystalline order. *Phys. Rev. A.* 38:1005–1018.

Skalak, R., A. Torzen, R. P. Zadra, and S. Chien. 1973. Strain energy function of red blood cell membranes. *Biophys. J.* 13:245–264.

Smith, G. S., E. B. Sirota, C. R. Safinya, and N. A. Clark. 1988. Structure of the L_α phases in a hydrated phosphatidylcholine multimembrane. *Phys. Rev. Lett.* 60:813–816.

Tocanne, J.-F., L. Dupou-Cézanne, and A. Lopez. 1994. Lateral diffusion of lipids in model and natural membranes. *Prog. Lipid Res.* 33:203–237.

Tsuchida, K., and I. Hatta. 1988. ESR studies on the ripple phase in multilamellar phospholipid bilayers. *Biochim. Biophys. Acta.* 945: 73–80.

Vaz, W. L. C., F. Goodsaid-Zalduondo, and K. Jakobson. 1984. Lateral diffusion of lipids and proteins in bilayer membranes. *FEBS Lett.* 174: 199–207.

Velikov, K., K. Danov, M. I. Angelova, C. Dietrich, and B. Pouligny. 1999. Motion of a massive particle attached to a spherical interface: statistical properties of the particle path. *Colloids Surfaces A.* 149:245–251.

Velikov, K., C. Dietrich, A. Hadjiisky, K. Danov, and B. Pouligny. 1997. Motion of a massive microsphere bound to a spherical vesicle. *Europhys. Lett.* 40:405–410.

Waugh, R. E. 1982a. Surface viscosity measurement from large bilayer vesicle tether formation. I. Analysis. *Biophys. J.* 38:19–27.

Waugh, R. E. 1982b. Surface viscosity measurement from large bilayer vesicle tether formation. II. Experiments. *Biophys. J.* 38:29–37.

Waugh, R. E., and E. A. Evans. 1979. Thermoelasticity of red blood cell membrane. *Biophys. J.* 26:115–132.

Wittebort, R. J., C. F. Schmidt, and R. G. Griffin. 1981. Solid-state carbon-13 nuclear magnetic resonance of the lecithin gel to liquid-crystalline phase transition. *Biochemistry.* 20:4223–4228.

Zhelev, D. V., D. Needham, and R. M. Hochmuth. 1994. A novel micropipet method for measuring the bending modulus of vesicle membranes. *Biophys. J.* 67:720–727.